Available online at www.sciencedirect.com
ScienceDirect
Journal of Computational Physics 224 (2007) 288–313
JOURNAL OF COMPUTATIONAL PHYSICS
www.elsevier.com/locate/jcp

A Darcy law for the drift velocity in a two-phase flow model

H. Guillard [a,*], F. Duval [b]

[a] INRIA, B.P. 93, 06902 Sophia Antipolis Cedex, France
[b] Institut de Radioprotection et de Sûreté Nucléaire (IRSN), BP3-13115 St. Paul-lez-Durance Cedex, France

Received 4 September 2006; received in revised form 9 February 2007; accepted 12 February 2007
Available online 12 March 2007

Abstract

This work deals with the design and numerical approximation of an Eulerian mixture model for the simulation of two-phase dispersed flows. In contrast to the more classical two-fluid or Drift-flux models, the influence of the velocity disequilibrium is taken into account through dissipative second-order terms characterized by a Darcy law for the relative velocity. As a result, the convective part of the model is always unconditionally hyperbolic. We show that this model corresponds to the first-order equilibrium approximation of classical two-fluid models. A finite volume approximation of this system taking advantage of the hyperbolic nature of the convective part of the model and of the particular structural form of the dissipative part is proposed. Numerical applications are presented to assess the capabilities of the model.

Keywords: Two-phase flows; Bubbly flows; Drift-flux; Riemann solver; Darcy law; Chapman–Enskog expansion

1. Introduction

Two-phase flows appear in a large number of engineering applications including the petroleum industry as well as industrial processes involving bubble column reactors (oxidation, hydrogenation, mixing of heterogeneous compositional materials, etc.). They also take an important place in the nuclear industry for reactors in operating conditions as well as in severe accident conditions. The macroscopic description of such flows is usually obtained by some averaging procedure [1–3], and is performed essentially by two large classes of models.

The first class that corresponds to the most general form obtained from the averaging procedure consists of separate mass, momentum and energy conservation equations written for each phase of the multiphase system. This corresponds to the well-known two-fluid model characterized in their most general form by two different velocities and pressures for each phase and possibly supplemented by topological equations [4,5] as well as the more classical one pressure, two velocity models whose closure is realized by the assumption of equality of the phase pressures [6–9].

* Corresponding author. Tel.: +33 04 92 38 77 96; fax: +33 04 92 38 79 80.
E-mail address: Herve.Guillard@sophia.inria.fr (H. Guillard).

0021-9991/$ - see front matter
doi:10.1016/j.jcp.2007.02.025

The second class of model corresponds to the mixture models and consists of single conservation equation for the mixture (mass, momentum and energy) and a mass conservation equation for one of the two phases. In this class, one can distinguish the so-called drift-flux models [10–13] for which an additional relation for the relative velocity is provided and the homogeneous models [14] that assumes a no-slip hydrodynamic law between the two phases. Some intermediate models have been proposed between these two large classes and we refer to [15,16] for some examples and to [3] for a presentation and a discussion of these models.

The two-fluid models are widely used for two-phase flow studies but have some drawbacks. The first difficulty concerns the modeling of interphase exchange terms. Indeed, there is a lot of practical situations for which the use of a two-fluid model requires an accurate modeling of the interfacial transfer terms (drag, lift, added mass, etc.) in order to capture correctly the two-phase flow behavior. Furthermore, from a mathematical point of view, it is well known that the one pressure two-fluid system is not unconditionally hyperbolic depending on the closure for interfacial terms. Finally from a numerical point of view, the complexity of the modeling, the presence of non-conservative products as well as the possible loss of hyperbolicity of the models make the approximation of these models difficult and dubious.

The mixture models are simpler and are expected to be well suited for situations where the two phases are well coupled. However, the mixture models also experience some difficulties. The homogeneous models are unable to take into account even a slight disequilibrium between the velocities of the phases and on the other hand, the drift-flux models have also some drawbacks. These drawbacks lie mainly in the constitutive relation for the drift velocity. First, the resulting system is not always hyperbolic. For instance, for two phases having different densities, both the Stokes and the Churn drift correlations leads to non-hyperbolic systems. The second weak point of this type of model is that the complexity of the drift-flux correlation sometimes prevents the existence of an analytical expression of the fluxes in terms of conservative variables and thus the approximation of these models requires complex and specialized methods [12,13].

In this paper, we examine situations where the two-phase flows are characterized by a stiff mechanical relaxation. By stiff mechanical relaxation, we mean a situation where the velocities of the two-phase tends towards a common value under the effects of the drag forces. In these situation, the use of homogeneous model is not always successful as even a slight velocity disequilibrium can have a large influence on the behavior of the system and it is often more accurate to be able to retain some non-equilibrium effects. We will show that this is possible in the framework of mixture model by deriving the first-order Chapman–Enskog asymptotic system corresponding to two-fluid models. In particular, we will show that the use of the Chapman–Enskog expansion allows to express the relative velocity between the phases by a Darcy law. Moreover, the resulting model is unconditionally hyperbolic and dissipative. This type of model offers therefore some advantages over the more classical two-fluid or drift-flux models. This paper is organized as follows: In the first section we recall in an isothermal setting the classical two-fluid model and show how to derive from it a reduced mixture model characterized by a Darcy law for the drift (relative) velocity. The second section is devoted to the mathematical analysis of this model. We will see that the convective part of the model is unconditionnaly hyperbolic in contrast to the more classical two-fluid or drift-flux model but also that it is dissipative and consistent. In the third section of this paper, we describe the numerical approximation of this system that we have used while the last section presents some numerical experiments.

2. A Darcy law for the drift velocity

2.1. The two-fluid multiphase model

We consider the well-known one pressure two-fluid model. Restricted to isothermal flows this model consists in separate mass and momentum conservation equations for each phase:

$$\frac{\partial \alpha_1 \rho_1}{\partial t} + \nabla \cdot (\alpha_1 \rho_1 \mathbf{v}_1) = 0, \tag{1}$$

$$\frac{\partial \alpha_1 \rho_1 \mathbf{v}_1}{\partial t} + \nabla \cdot (\alpha_1 \rho_1 \mathbf{v}_1 \otimes \mathbf{v}_1) + \nabla(\alpha_1 p) = p_I \nabla \alpha_1 + \mathbf{F}^d + \alpha_1 \rho_1 \mathbf{g}, \tag{2}$$

$$\frac{\partial \alpha_2 \rho_2}{\partial t} + \nabla \cdot (\alpha_2 \rho_2 \mathbf{v}_2) = 0, \tag{3}$$

$$\frac{\partial \alpha_2 \rho_2 \mathbf{v}_2}{\partial t} + \nabla \cdot (\alpha_2 \rho_2 \mathbf{v}_2 \otimes \mathbf{v}_2) + \nabla(\alpha_2 p) = p_I \nabla \alpha_2 - \mathbf{F}^d + \alpha_2 \rho_2 \mathbf{g}. \tag{4}$$

The notations are classicals. α_k are the volume fractions of each phase ($\alpha_1 + \alpha_2 = 1$), ρ_k the phase densities, $\mathbf{v}_k$ the vector velocities and p the common pressure of the two phases.

On the right-hand side of Eqs. (2) and (4) appear some terms related to averaged momentum exchanges between the two phases. We have focussed here on the drag force $\mathbf{F}^d$ and the non-conservative term $p_I \nabla \alpha_k$ where p_I denotes the macroscopic interfacial pressure. The drag force may be written as the following pseudo-linear constitutive relation:

$$\mathbf{F}^d = \lambda(\mathbf{v}_2 - \mathbf{v}_1). \tag{5}$$

This represents the simplest form fulfilling the entropy inequality [2]. The coefficient λ is a positive scalar that may depend on the characteristics of each phase (including the relative velocity). This parameter represents the drag coefficient for which there exist a large number of correlations [17,18] and can be viewed as a velocity relaxation parameter controlling the rate at which the two velocities tend towards equilibrium. In this sense, we will see that it plays a key role in deriving reduced models. The macroscopic interfacial pressure p_I remains also to be specified to close the two-fluid model. Several estimates have been proposed for this interfacial pressure and we refer to [6–9] for some practical examples and their impact on the hyperbolicity of the system.

To close completely the system of the four equations (1)–(4), we must provide thermodynamical models for the two phases. Here, we consider a slightly compressible liquid phase for which the equation of state is written as:

$$p_1(\rho_1) = p_0 + a_1^2(\rho_1 - \rho_L), \tag{6}$$

where p_0 denotes some constant reference pressure. The constants ρ_L and a_1 are the corresponding density and velocity of sound at this reference state. For the gas phase, we adopt the perfect gas equation of state:

$$p_2(\rho_2) = \rho_2 a_2^2. \tag{7}$$

The pressure p is found by putting $p_1 = p_2 = p$ in the two equation of states and then solving the equation:

$$\frac{\alpha_1 \rho_1}{\rho_1(p)} + \frac{\alpha_2 \rho_2}{\rho_2(p)} = 1. \tag{8}$$

Introducing the mixture density $\rho = \alpha_1 \rho_1 + \alpha_2 \rho_2$ and the mass gas fraction of the gas by $\alpha_2 \rho_2 = \rho Y$ and taking the positive root of (8), the pressure is given by:

$$p(\rho, \rho Y) = \frac{z}{2} + \frac{1}{2}\sqrt{z^2 - 4\rho Y a_2^2(p_0 - a_1^2 \rho_L)} \tag{9}$$

with:

$$z = (p_0 - a_1^2 \rho_L) + \rho(Y a_2^2 + (1 - Y)a_1^2). \tag{10}$$

As stated in Section 1, the two-fluid model (1)–(4) may appear to be too complex for situations in which the two phases are strongly coupled. This is the case for instance for a large range of dispersed two-phase flows for which simpler models such as mixture models produce accurate results [10]. In this case, one can use simpler or reduced models involving a mixture velocity rather than two independent ones. Indeed, this allows to reduce greatly the modeling issue by avoiding the closure of average interphase momentum exchanges (interfacial pressure, added mass, lift and Basset forces, etc.). From a numerical point of view this also greatly reduces the complexity by not only avoiding the discretization of the interaction terms but also by reducing the number of waves and their treatment.

Our aim, in this paper, is to derive such a reduced mixture model while still retaining some dynamical effects linked to the velocity disequilibrium $\mathbf{v}_1 \neq \mathbf{v}_2$. We will do that by considering situations for which the drag coefficient λ is large (but not infinite) and consider the first-order in $1/\lambda$ asymptotic equilibrium model. Indeed, it is well known that for certain physical situations such as detonation in granular media [16], the drag coefficient

can become very high, typically $\lambda \geqslant 10^{10}\ \mathrm{kg\,m^{-3}\,s^{-1}}$. For dispersed two-phase bubbly flows this coefficient is also expected to be large or in other words the drag terms are expected to be the dominant ones. This can be viewed by writing the two-fluid model (1)–(4) in a dimensionless form. Introducing the dimensionless quantities as $\tilde{\phi} = \phi/\phi^*$ where ϕ^* denotes some reference value, the dimensionless two-fluid model can be written as:

$$\frac{\partial \alpha_1 \tilde{\rho}_1}{\partial \tilde{t}} + \tilde{\nabla} \cdot (\alpha_1 \tilde{\rho}_1 \tilde{\mathbf{v}}_1) = 0, \tag{11}$$

$$\frac{\partial \alpha_1 \tilde{\rho}_1 \tilde{\mathbf{v}}_1}{\partial \tilde{t}} + \tilde{\nabla} \cdot (\alpha_1 \tilde{\rho}_1 \tilde{\mathbf{v}}_1 \otimes \tilde{\mathbf{v}}_1) = -Eu \alpha_1 \tilde{\nabla} \tilde{p} + Dr \tilde{\lambda} \tilde{\mathbf{v}}_r + \frac{\alpha_1 \tilde{\rho}_1}{Fr} \frac{\mathbf{g}}{\|\mathbf{g}\|}, \tag{12}$$

$$\frac{\partial \alpha_2 \tilde{\rho}_2}{\partial \tilde{t}} + \tilde{\nabla} \cdot (\alpha_2 \tilde{\rho}_2 \tilde{\mathbf{v}}_2) = 0, \tag{13}$$

$$\frac{\partial \alpha_2 \tilde{\rho}_2 \tilde{\mathbf{v}}_2}{\partial \tilde{t}} + \tilde{\nabla} \cdot (\alpha_2 \tilde{\rho}_2 \tilde{\mathbf{v}}_2 \otimes \tilde{\mathbf{v}}_2) = -Eu \alpha_2 \tilde{\nabla} \tilde{p} - Dr \tilde{\lambda} \tilde{\mathbf{v}}_r + \frac{\alpha_2 \tilde{\rho}_2}{Fr} \frac{\mathbf{g}}{\|\mathbf{g}\|}. \tag{14}$$

Here, for the sake of simplicity, we have assumed that the macroscopic interfacial pressure is equal to the common pressure of the two phases. $Eu = p^*/\rho^* \mathbf{v}^{*2}$ denotes the Euler number related to the Mach number by $Eu = 1/\mathrm{M}^2$ where ρ^* and $\mathbf{v}^*$ correspond, respectively, to some reference density and velocity. $Fr = \mathbf{v}^{*2}/\|\mathbf{g}\|L^*$ is the Froude number and Dr is a dimensionless "drag number" defined by:

$$Dr = \frac{L^* \lambda^* \mathbf{v}_r^*}{\rho^* \mathbf{v}^{*2}}. \tag{15}$$

At this point, to continue the analysis, an estimate for the reference drag coefficient λ^* has to be specified. For dispersed two-phase flows, a large number of correlations are available (see for instance [18] for a review). Most of them consist in writing the coefficient λ as:

$$\lambda = \frac{3}{8r} \alpha_2 C_{\mathrm{D}} \rho_1 \|\mathbf{v}_r\|, \tag{16}$$

where C_{D} is a dimensionless drag coefficient and r is the average radius of the bubbles. Hence, expression (16) allows to identify the reference drag coefficient and to write the Drag number as:

$$Dr = \frac{3}{8} \frac{L^*}{r^*} C_{\mathrm{D}} \left(\frac{\mathbf{v}_r^*}{\mathbf{v}^*} \right)^2. \tag{17}$$

For most bubbly flows, it seems to be reasonable to assume that the relative velocity is of the same order of magnitude than the phase velocities and thus it is legitimate to assume that the reference velocities $\mathbf{v}_r^*$ and $\mathbf{v}^*$ are of the same order of magnitude. This means that the drag number is driven by the ratio of the macroscopic characteristic length L^* and the microscopic one r^* which is expected to be very high for dispersed flows. To illustrate this order of magnitude analysis let us consider the typical cases of a nuclear reactor that is several meters high: $L^* = \mathcal{O}(1)$ m. In these devices, the radius of the vapor bubbles are of the order of the millimeter: $r^* = \mathcal{O}(10^{-3})$ m while their velocities is of the order of $v^* = \mathcal{O}(10^{-1})$ m/s. With the usual values of the gravity constant we thus get $Fr^{-1} \sim Dr \sim 10^3$ while on the other hand the Euler number is of the order of $Eu = (a^*/v^*)^2$ where a^* is some typical speed of sound and is therefore expected to be at least of the same order of magnitude. This order of magnitude analysis thus illustrates that the three terms on the right-hand side of the momentum equations are the dominant ones.

2.2. Chapman–Enskog derivation of the Darcy drift model

In this section, we derive the first-order asymptotic equilibrium system corresponding to large values of λ in the system (1)–(4). We model this situation by setting $\lambda = \lambda'/\epsilon$ with $\lambda' = \mathcal{O}(1)$ and let $\epsilon \to 0$. Therefore, we expect the two-phase velocities $\mathbf{v}_1$ and $\mathbf{v}_2$ to differ by a factor of order ϵ and thus introduce the Chapman–Enskog expansion

$$\mathbf{v}_1 = \mathbf{v}^0 + \epsilon \mathbf{v}_1^1 + \mathcal{O}(\epsilon^2), \tag{18}$$

$$\mathbf{v}_2 = \mathbf{v}^0 + \epsilon \mathbf{v}_2^1 + \mathcal{O}(\epsilon^2) \tag{19}$$

into the system (1)–(4) to obtain

Proposition 1. *Assume that the interface pressure* $p_I = p + \mathcal{O}(\epsilon)$, *then the first order asymptotic equilibrium system is given by*

$$\frac{\partial \rho^0}{\partial t} + \nabla \cdot (\rho^0 \mathbf{v}^0) = 0, \tag{20}$$

$$\frac{\partial \rho^0 \mathbf{v}^0}{\partial t} + \nabla \cdot (\rho^0 \mathbf{v}^0 \otimes \mathbf{v}^0) + \nabla p^0 = \rho^0 \mathbf{g}, \tag{21}$$

$$\frac{\partial \rho^0 Y^0}{\partial t} + \nabla \cdot (\rho^0 \mathbf{v}^0 Y^0) = -\nabla \cdot (\rho^0 Y^0 (1 - Y^0) \mathbf{v}_r^0), \tag{22}$$

where the relative velocity $\mathbf{v}_r^0$ *is given by the relation*

$$\lambda \mathbf{v}_r^0 = \alpha_1^0 \alpha_2^0 \frac{\rho_2^0 - \rho_1^0}{\rho^0} \nabla p^0. \tag{23}$$

Proof. In the case of conservative system, a full description of the Chapman–Enskog methodology can be found in [19]. Although the system (1)–(4) is not in conservative form, the adaptation of this technique to this system is easy and is left to the reader. The equilibrium state (denoted here by the superscript 0) is totally characterized by the two-phase masses $(\alpha_1\rho_1)^0$, $(\alpha_2\rho_2)^0$ and the mixture momentum $(\rho\mathbf{v})^0$ or alternatively by the variables $\rho^0, Y^0, \mathbf{v}^0$. Now, assume that at any point $\mathbf{x}$ and time t of the domain of interest, the conservative variables $\rho, \rho Y, \rho\mathbf{v}$ are known. According to the Chapman–Enskog methodology (see [19]), the equilibrium state is required to match these values

$$\rho = (\alpha_1\rho_1)^0 + (\alpha_2\rho_2)^0, \tag{24}$$

$$\rho Y = (\alpha_2\rho_2)^0, \tag{25}$$

$$\rho\mathbf{v} = (\rho\mathbf{v})^0 \tag{26}$$

then, using the expansions

$$\rho = \rho^0 + \epsilon\rho^1 + \mathcal{O}(\epsilon^2), \tag{27}$$

$$Y = Y^0 + \epsilon Y^1 + \mathcal{O}(\epsilon^2), \tag{28}$$

$$\mathbf{v}_k = \mathbf{v}^0 + \epsilon\mathbf{v}_k^1 + \mathcal{O}(\epsilon^2) \tag{29}$$

the following relationships are obtained

$$\rho^1 = 0, \tag{30}$$

$$Y^1 = 0, \tag{31}$$

$$Y^0\mathbf{v}_2^1 + (1 - Y^0)\mathbf{v}_1^1 = 0. \tag{32}$$

Next, introducing the expansion (18), (19) into (2) and (4), we obtain

$$(\alpha_1\rho_1)^0 \frac{\mathrm{D}\mathbf{v}^0}{\mathrm{D}t} + \nabla(\alpha_1^0 p^0) = p^0 \nabla\alpha_1^0 + \lambda'(\mathbf{v}_2^1 - \mathbf{v}_1^1) + (\alpha_1\rho_1)^0\mathbf{g} + \mathcal{O}(\epsilon), \tag{33}$$

$$(\alpha_2\rho_2)^0 \frac{\mathrm{D}\mathbf{v}^0}{\mathrm{D}t} + \nabla(\alpha_2^0 p^0) = p^0 \nabla\alpha_2^0 - \lambda'(\mathbf{v}_2^1 - \mathbf{v}_1^1) + (\alpha_2\rho_2)^0\mathbf{g} + \mathcal{O}(\epsilon). \tag{34}$$

Multiplying (33) by $(\alpha_2\rho_2)^0$ and (34) by $(\alpha_1\rho_1)^0$ and taking the difference of the two equations we get

$$\lambda'(\mathbf{v}_2^1 - \mathbf{v}_1^1) = \alpha_1^0\alpha_2^0 \frac{\rho_2^0 - \rho_1^0}{\rho^0} \nabla p^0 + \mathcal{O}(\epsilon). \tag{35}$$

This relation together with (32) can be solved to obtain the expression of $\mathbf{v}_1^1$ and $\mathbf{v}_2^1$. Introducing these expressions in (1)–(4) results in the system (20)–(22). □

The relation (35) is reminiscent of the Darcy law used in the study of porous media. However, it holds here for the relative velocity $\mathbf{v}_2 - \mathbf{v}_1$ while in porous media, the Darcy law is used to define the fluid velocity. Relation (35) has already been obtained in [3] but seems to have been largely unexploited in the two-phase flow literature. We also note that the previous proof shows that the diffusive velocities $\mathbf{v}_k - \mathbf{v}$ have to be taken into account in the partial mass conservation equation but that they can be neglected in the mixture momentum equation where they represent a correction of order $\mathcal{O}(\epsilon)^2$. This is in contrast with drift-flux models where the influence of the drift velocity is retained in the momentum equation. We finally remark that the assumption on the interface pressure is usually verified since the standard models for the interface pressure [7–9] are of the form $p_I = p + \beta\|\mathbf{v}_r\|^2$ where β is some coefficient that does not depend on the drift velocity.

2.3. Connections with drift-flux models

In the engineering literature, a large number of experimental or empirical correlations where the relative velocity $\mathbf{v}_r$ is expressed under the form of an algebraic expression are proposed [17,18]. The purpose of this section is to show the connection of these models with the Darcy drift approximation:

$$\lambda \mathbf{v}_r = \alpha_1\alpha_2 \frac{\rho_2 - \rho_1}{\rho} \nabla p. \tag{36}$$

For instance in laminar flows, in the so-called Stokes regime, the relative velocity of small particles is given by the well-known formula (see [2], formula X.2.13)

$$\mathbf{v}_r = \frac{2\alpha_1^2 r^2}{9\mu_1}(\rho_1 - \rho_2)\mathbf{g}, \tag{37}$$

where μ_1 is the viscosity of the liquid and r denotes some effective radius of the particles. On the other hand, for dispersed flows, the drag force is usually expressed by the formula (16)

$$\mathbf{F}^d = \frac{3\alpha_2}{8r} C_D \rho_1 \|\mathbf{v}_r\|\mathbf{v}_r, \tag{38}$$

where the dimensionless drag coefficient C_D is an empirical parameter that depends on the characteristics of the flow. This coefficient C_D is usually given as a function of α_2 and the bubble Reynolds number R_e defined by:

$$R_e = 2r\rho_1\|\mathbf{v}_r\|/\mu_m = 2r\alpha_1\rho_1\|\mathbf{v}_r\|/\mu_1, \tag{39}$$

where we have used the standard estimates $\mu_m = \mu\alpha_1^{-1}$ for the viscosity of the mixture. For instance, in the Stokes regime $R_e \leqslant 2$, the drag coefficient is given by $C_D = 24/R_e$. This gives the following expression for the drag coefficient λ

$$\lambda = \frac{9\alpha_2\mu_1}{2\alpha_1 r^2}. \tag{40}$$

Assuming that the pressure is in hydrostatic equilibrium

$$\nabla p = -\rho\mathbf{g}. \tag{41}$$

The Darcy drift law (36) together with (40) exactly gives the drift correlation (37). Actually under the assumption of hydrostatic equilibrium, the Darcy drift law (36) allows to recover a large number of algebraic drift correlations known in the engineering literature. We refer here to [20] where a large number of empirical correlations are reviewed for a study of the relationship between the expression of the drag coefficient C_D and usual algebraic drift correlations.

3. Mathematical properties

In this section, we discard the external forces and study the differential part of the system. The system being invariant by rotation, the developments will be performed in the one-dimensional case. We will use $\mathbf{Q} = (\rho, \rho u, \rho Y)^t$ as the state vector of conservative variables and write the system (20)–(22) under the form:

$$\frac{\partial \mathbf{Q}}{\partial t}+\frac{\partial \mathscr{F}(\mathbf{Q})}{\partial x}=\frac{\partial \mathscr{D}(\mathbf{Q},\nabla\mathbf{Q})}{\partial x}, \tag{42}$$

where $\mathscr{F}(\mathbf{Q})$ and $\mathscr{D}(\mathbf{Q},\nabla\mathbf{Q})$ denote, respectively, the "convective" and "diffusive" fluxes.

3.1. Existence of a mathematical entropy

Proposition 2. *Let $f_k(\rho_k)$ be the specific free energy of each phase verifying $f_k'(\rho_k)=p_k/\rho_k^2$ and let the pair (η,G) be defined by*:

$$\eta(\mathbf{Q})=\frac{\rho\mathbf{v}^2}{2}+\sum_k \alpha_k\rho_k f_k(\rho_k),\quad G(\mathbf{Q})=(\eta+p)\mathbf{v}. \tag{43}$$

Then (η,G) is an entropy–flux pair for the system (20)–(22).

Proof. The system being invariant by rotation, it is sufficient to consider the one-dimensional case. For the pair (η,G) given by (43), we must verify the relation:

$$\nabla_{\mathbf{Q}}\eta(\mathbf{Q})^{\mathrm{t}}\cdot\mathbf{A}(\mathbf{Q})=\nabla_{\mathbf{Q}}G(\mathbf{Q})^{\mathrm{t}}, \tag{44}$$

where $\mathbf{A}(\mathbf{Q})$ is the jacobian matrix $\partial\mathscr{F}(\mathbf{Q})/\partial\mathbf{Q}$ given by:

$$\mathbf{A}(\mathbf{Q})=\begin{pmatrix} 0 & 1 & 0\\ -u^2+\left(\frac{\partial p}{\partial\rho}\right)_{\rho Y} & 2u & \left(\frac{\partial p}{\partial\rho Y}\right)_{\rho}\\ -uY & Y & u\end{pmatrix}. \tag{45}$$

Hence, the first step consists in computing $\nabla_{\mathbf{Q}}\eta(\mathbf{Q})$. From the expression (43) for the function $\eta(\mathbf{Q})$ one has:

$$\left(\frac{\partial\eta(\mathbf{Q})}{\partial\rho}\right)_{\rho u,\rho Y}=-\frac{u^2}{2}+g_1(\rho_1,p), \tag{46}$$

$$\left(\frac{\partial\eta(\mathbf{Q})}{\partial\rho u}\right)_{\rho,\rho Y}=u, \tag{47}$$

$$\left(\frac{\partial\eta(\mathbf{Q})}{\partial\rho Y}\right)_{\rho,\rho u}=g_2(\rho_2,p)-g_1(\rho_1,p), \tag{48}$$

where $g_k(\rho_k,p)=f_k(\rho_k)+p/\rho_k$ denotes the specific Gibbs free energy of each phase. On the other hand, estimating the derivatives on the right-hand side of (44) leads to:

$$\left(\frac{\partial G(\mathbf{Q})}{\partial\rho}\right)_{\rho u,\rho Y}=u\left[\left(\frac{\partial\eta(\mathbf{Q})}{\partial\rho}\right)_{\rho u,\rho Y}+\left(\frac{\partial p}{\partial\rho}\right)_{\rho Y}\right]-\frac{u}{\rho}[\eta(\mathbf{Q})+p], \tag{49}$$

$$\left(\frac{\partial G(\mathbf{Q})}{\partial\rho u}\right)_{\rho,\rho Y}=u^2+\frac{1}{\rho}[\eta(\mathbf{Q})+p], \tag{50}$$

$$\left(\frac{\partial G(\mathbf{Q})}{\partial\rho Y}\right)_{\rho,\rho u}=u\left[\left(\frac{\partial\eta(\mathbf{Q})}{\partial\rho Y}\right)_{\rho,\rho u}+\left(\frac{\partial p}{\partial\rho Y}\right)_{\rho}\right]. \tag{51}$$

At this point we are in position to verify the equality (44). Developing the product of the left-hand side of (44) shows easily that the relation (44) is verified and this completes the proof. □

3.2. Consistency of the entropy with second order terms

Proposition 3. *$\eta(\mathbf{Q})$ is an entropy for the system consistent with second order terms.*

The consistency of the entropy with second order terms means that there exists three regular functions $G(\mathbf{Q})$, $H(\mathbf{Q},\nabla\mathbf{Q})$ and $S(\mathbf{Q})$ such that $\eta(\mathbf{Q})$ satisfies the additional conservation law:

$$\frac{\partial \eta(\mathbf{Q})}{\partial t} + \nabla \cdot G(\mathbf{Q}) = \nabla \cdot H(\mathbf{Q}, \nabla \mathbf{Q}) + S(\mathbf{Q}), \tag{52}$$

where $G(\mathbf{Q})$ is the entropy flux defined by (44) and where $S(\mathbf{Q}) \leqslant 0$. The proof of this result is as follows

Proof. Again, the system being invariant by rotation, the proof can be done by considering only the one-dimensional case. Since $\mathbf{Q}$ satisfies the system

$$\frac{\partial \mathbf{Q}}{\partial t} + \frac{\partial \mathscr{F}(\mathbf{Q})}{\partial x} = \frac{\partial \mathscr{D}(\mathbf{Q}, \nabla \mathbf{Q})}{\partial x} \tag{53}$$

then $\eta(\mathbf{Q})$ is solution of the equation:

$$\frac{\partial \eta(\mathbf{Q})}{\partial t} + \nabla_{\mathbf{Q}} \eta(\mathbf{Q}) \cdot \frac{\partial \mathscr{F}(\mathbf{Q})}{\partial x} = \frac{\partial \nabla_{\mathbf{Q}} \eta(\mathbf{Q}) \cdot \mathscr{D}(\mathbf{Q}, \nabla \mathbf{Q})}{\partial x} - \frac{\partial \nabla_{\mathbf{Q}} \eta(\mathbf{Q})}{\partial x} \cdot \mathscr{D}(\mathbf{Q}) \tag{54}$$

the second term on the left-hand side of this equation has been shown to be equal to $\partial G(\mathbf{Q})/\partial x$ in Proposition 2 and thus it remains to prove that $\partial \nabla_{\mathbf{Q}} \eta(\mathbf{Q})/\partial x \cdot \mathscr{D}(\mathbf{Q})$ is a positive term. We first note that we have:

$$\nabla g_k(\rho_k, p) = \frac{1}{\rho_k} \nabla p. \tag{55}$$

This leads to:

$$\frac{\partial \nabla_{\mathbf{Q}} \eta(\mathbf{Q})}{\partial x} \cdot \mathscr{D}(\mathbf{Q}) = \frac{\partial}{\partial x}(g_2(\rho_2, p) - g_1(\rho_1, p))\rho Y(1 - Y)\mathbf{v}_r = \frac{1}{\lambda} \alpha_1^2 \alpha_2^2 \frac{(\rho_2 - \rho_1)^2}{\rho^2} (\nabla p)^2 \tag{56}$$

and this completes the proof. □

The previous result is important because it establishes that the Darcy drift model has a dissipative effect: this model of the drift velocity allows a control of the total energy of the flow:

Corollary 4. *Let Ω be a closed system, that is $\mathbf{n} \cdot \mathbf{v} = 0$ and $\mathbf{n} \cdot \nabla p = 0$ where $\mathbf{n}$ denotes the outward-directed normal at the boundary $\partial\Omega$ and define $\mathscr{N}$ the total energy on Ω by*:

$$\mathscr{N} = \int_{\Omega} \eta(\mathbf{Q}). \tag{57}$$

Then $\mathscr{N}$ is a decreasing function of time.

3.3. Hyperbolicity

Let us write the system (20)–(22) under the compact notation (53). In this section we discard the diffusive terms and concentrate on the first-order part of the system:

$$\frac{\partial \mathbf{Q}}{\partial t} + \frac{\partial \mathscr{F}(\mathbf{Q})}{\partial x} = 0. \tag{58}$$

We will prove that the system (58) is unconditionally hyperbolic. To do that, we show that this system is symmetrizable. The system being invariant by rotation, this study will be performed in one dimension for the sake of simplicity.

Proposition 5. *Let $\mathbf{q} = (p, \mathbf{v}, Y)^t$ then the transformation $\mathbf{q} \leftrightarrow \mathbf{Q}$ is a one-to-one mapping*

Proof. This results from simple algebraic computations □

Proposition 6. *The system is symmetrizable*

Proof. We show below that the system written in term of the non-conservative variables $\mathbf{q}$ is symmetric and can be written

$$\mathbf{M}(\mathbf{q})\frac{\partial \mathbf{q}}{\partial t}+\mathbf{B}(\mathbf{q})\frac{\partial \mathbf{q}}{\partial x}=0, \tag{59}$$

where $\mathbf{M}(\mathbf{q})$ is symmetric definite positive and $\mathbf{B}(\mathbf{q})$ is a symmetric matrix.

Since, the evolution equation for the variables $\mathbf{v}$ and Y are obvious, it just remains to establish the evolution equation for the pressure. For this aim, we first express the partial derivatives of the pressure with respect to the conservative variables that are obtained by using extensively the equality of the two pressures. From this equality and the barotropic equation of state for each phase $p_k = p_k(\rho_k)$, one can write:

$$\mathrm{d}p=\frac{a_1^2}{2}\,\mathrm{d}\rho_1+\frac{a_2^2}{2}\,\mathrm{d}\rho_2. \tag{60}$$

Next, using the relations $\rho_1=(\rho-\rho Y)/\alpha_1$ and $\rho_2=\rho Y/\alpha_2$ leads to:

$$\mathrm{d}p=\frac{a_1^2}{2\alpha_1}\,\mathrm{d}\rho+\frac{\alpha_1 a_2^2-\alpha_2 a_1^2}{2\alpha_1\alpha_2}\,\mathrm{d}(\rho Y)+\frac{\alpha_2\rho_1 a_1^2-\alpha_1\rho_2 a_2^2}{2\alpha_1\alpha_2}\,\mathrm{d}\alpha_2. \tag{61}$$

At this point, it remains to express the last term on the right-hand side of Eq. (61) as a function of conservative variable differentials. This can be done by using a similar route. From $p_1=p_2$ one can write $a_1^2\,\mathrm{d}\rho_1=a_2^2\,\mathrm{d}\rho_2$, and then introducing again the relations $\rho_k=\rho Y_k/\alpha_k$ leads to:

$$\mathrm{d}\alpha_2=\frac{1}{\alpha_2\rho_1 a_1^2+\alpha_1\rho_2 a_2^2}[-a_1^2\alpha_2\mathrm{d}\rho+(\alpha_1 a_2^2+\alpha_2 a_1^2)\mathrm{d}(\rho Y)]. \tag{62}$$

This allows to obtain the partial derivatives of the pressure using the set of conservative variables $(\rho,\rho Y)$ which are thus given by:

$$\left(\frac{\partial p}{\partial \rho}\right)_{\rho Y}=\frac{\rho a^2}{\rho_1}, \tag{63}$$

$$\left(\frac{\partial p}{\partial \rho Y}\right)_{\rho}=\frac{\rho a^2(\rho_1-\rho_2)}{\rho_1\rho_2}, \tag{64}$$

where a denotes the average sound speed which is defined by:

$$\frac{1}{\rho a^2}=\sum_k\frac{\alpha_k}{\rho_k a_k^2}. \tag{65}$$

Hence, defining the Lagrangian derivative of a quantity ϕ by $\frac{\mathrm{D}\phi}{\mathrm{D}t}=\frac{\partial\phi}{\partial t}+\mathbf{v}\cdot\nabla\phi$ we have:

$$\frac{\mathrm{D}p}{\mathrm{D}t}=\rho a^2\left[\frac{1}{\rho_1}\frac{\mathrm{D}\rho}{\mathrm{D}t}+\left(\frac{1}{\rho_2}-\frac{1}{\rho_1}\right)\frac{\mathrm{D}\rho Y}{\mathrm{D}t}\right]=-\rho a^2\left[\frac{1}{\rho_1}\rho+\left(\frac{1}{\rho_2}-\frac{1}{\rho_1}\right)\rho Y\right]\nabla\cdot\mathbf{v}=-\rho a^2\nabla\cdot\mathbf{v}. \tag{66}$$

Thus the system can be written in the symmetrized form (59) where the matrices $\mathbf{M}(\mathbf{q})$ and $\mathbf{B}(\mathbf{q})$ are defined by:

$$\mathbf{M}(\mathbf{q})=\begin{pmatrix}1/(\rho a^2) & 0 & 0\\ 0 & 1/\rho & 0\\ 0 & 0 & 1\end{pmatrix},\quad \mathbf{B}(\mathbf{q})=\begin{pmatrix}u/(\rho a^2) & 1 & 0\\ 1 & u/\rho & 0\\ 0 & 0 & u\end{pmatrix} \tag{67}$$

since the matrix $\mathbf{M}(\mathbf{q})$ is obviously definite positive and $\mathbf{B}$ is a symmetric matrix, we conclude that the system is symmetrizable and thus that it is hyperbolic. □

3.4. Eigenstructure

These computations will be done using the set of non-conservative variables $\mathbf{q}=(p,\mathbf{v},Y)^{\mathrm{t}}$. According to the previous result, in these variables, the system writes in matricial form as:

$$\frac{\partial \mathbf{q}}{\partial t}+\mathbf{A}(\mathbf{q})\frac{\partial \mathbf{q}}{\partial x}=0, \tag{68}$$

where the jacobian $\mathbf{A}(\mathbf{q})$ is given by:

$$\mathbf{A}(\mathbf{q}) = \mathbf{M}^{-1}(\mathbf{q})\mathbf{B}(\mathbf{q}) = \begin{pmatrix} u & \rho a^2 & 0 \\ \rho^{-1} & u & 0 \\ 0 & 0 & u \end{pmatrix}. \tag{69}$$

The matrix $\mathbf{A}$ admits three distinct eigenvalues given by:

$$\lambda_1(\mathbf{q}) = u - a, \quad \lambda_2(\mathbf{q}) = u, \quad \lambda_3(\mathbf{q}) = u + a. \tag{70}$$

The corresponding right eigenvectors $\mathbf{r}_k(\mathbf{q})$ for $k = 1, 2, 3$ are defined by $\mathbf{A}(\mathbf{q})\mathbf{r}_k(\mathbf{q}) = \lambda_k \mathbf{r}_k(\mathbf{q})$ and can be chosen as:

$$\mathbf{r}_1(\mathbf{q}) = \begin{pmatrix} -\rho a \\ 1 \\ 0 \end{pmatrix}, \quad \mathbf{r}_2(\mathbf{q}) = \begin{pmatrix} 0 \\ 0 \\ 1 \end{pmatrix}, \quad \mathbf{r}_3(\mathbf{q}) = \begin{pmatrix} \rho a \\ 1 \\ 0 \end{pmatrix}. \tag{71}$$

The left eigenvectors $\mathbf{l}_k(\mathbf{q})$ for $k = 1, 2, 3$ are defined by $\mathbf{l}_k(\mathbf{q})\mathbf{A}(\mathbf{q}) = \lambda_k \mathbf{l}_k(\mathbf{q})$ and are given after the normalization $\mathbf{l}_i^t(\mathbf{q})\mathbf{r}_j(\mathbf{q}) = \delta_{ij}$:

$$\mathbf{l}_1(\mathbf{q}) = \begin{pmatrix} -1/2\rho a \\ 1/2 \\ 0 \end{pmatrix}, \quad \mathbf{l}_2(\mathbf{q}) = \begin{pmatrix} 0 \\ 0 \\ 1 \end{pmatrix}, \quad \mathbf{l}_3(\mathbf{q}) = \begin{pmatrix} 1/2\rho a \\ 1/2 \\ 0 \end{pmatrix}. \tag{72}$$

Proposition 7. *Let a_k be the speed of sound in phase k and assume that $\psi_k = (\partial a_k/\partial p)_Y > 0$ then the characteristic fields associated to the waves $\lambda_1(\mathbf{q}) = u - a$ and $\lambda_3(\mathbf{q}) = u + a$ are genuinely nonlinear, that is they verify $\nabla_{\mathbf{q}}\lambda_k(\mathbf{q}) \cdot \mathbf{r}_k(\mathbf{q}) \neq 0$ for $k = 1, 3$ for any admissible state $\mathbf{q}$.*

Proof. From the eigenvalues (70) and the right eigenvectors (71) one has:

$$\nabla_{\mathbf{q}}\lambda_1(\mathbf{q}) \cdot \mathbf{r}_1(\mathbf{q}) = \nabla_{\mathbf{q}}\lambda_3(\mathbf{q}) \cdot \mathbf{r}_3(\mathbf{q}) = 1 + \rho a \left(\frac{\partial a}{\partial p}\right)_{u,Y}. \tag{73}$$

Hence, to complete the proof, an expression for the average sound speed derivative must be provided. We use here similar developments as those performed in [15] by first writing the partial derivative of the sound speed of the mixture as:

$$\left(\frac{\partial a}{\partial p}\right)_Y = -a\left[\frac{(\rho a)^2}{2}\left(\frac{\partial 1/(\rho a)^2}{\partial p}\right)_Y - \rho\left(\frac{\partial (1/\rho)}{\partial p}\right)_Y\right]. \tag{74}$$

Next, the density and the sound speed of the mixture are rewritten as:

$$\frac{1}{\rho} = \sum\nolimits_k \frac{Y_k}{\rho_k}, \tag{75}$$

$$\frac{1}{(\rho a)^2} = \sum\nolimits_k \frac{Y_k}{(\rho_k a_k)^2}. \tag{76}$$

It follows that:

$$\left(\frac{\partial 1/(\rho a)^2}{\partial p}\right)_Y = -2\sum_k \frac{a_k Y_k (1 + \rho_k a_k \psi_k)}{(\rho_k a_k)^3}, \tag{77}$$

$$\left(\frac{\partial (1/\rho)}{\partial p}\right)_Y = -\frac{1}{(\rho a)^2}, \tag{78}$$

where the coefficients ψ_k are defined by $\psi_k = (\partial a_k/\partial p)_Y$. Hence, using Eqs. (77) and (78) together with Eq. (74) leads to:

$$1 + \rho a\left(\frac{\partial a}{\partial p}\right)_{u,Y} = (\rho a)^2 \sum_k \frac{a_k Y_k (1 + \rho_k a_k \psi_k)}{(\rho_k a_k)^3}. \tag{79}$$

As indicated in [15], it is legitimate to assume that the phase sound speed a_k increases with the pressure, that is $\psi_k > 0$, and thus when looking at Eq. (79) this complete the proof. □

Proposition 8. *The characteristic field associated to the wave $\lambda_2(\mathbf{q}) = u$ is linearly degenerate, that is it verifies $\nabla_{\mathbf{q}}\lambda_2(\mathbf{q}) \cdot \mathbf{r}_2(\mathbf{q}) = 0$ for any admissible state $\mathbf{q}$.*

Proof. From the eigenvalue $\lambda_2(\mathbf{q}) = u$ one has $\nabla_{\mathbf{q}}\lambda_2(\mathbf{q}) = (0, 1, 0)^{\mathrm{t}}$ and thus from the expression (71) for the right eigenvector $\mathbf{r}_2(\mathbf{q})$ one deduce easily $\nabla_{\mathbf{q}}\lambda_2(\mathbf{q}) \cdot \mathbf{r}_2(\mathbf{q}) = 0$. □

3.5. Riemann's invariants

We compute in this section the Riemann's invariants w of the system which are defined by: $\nabla_{\mathbf{q}} w(\mathbf{q}) \cdot \mathbf{r}_k(\mathbf{q}) = 0$.

We first begin with the Riemann's invariants associated to the eigenvalue $\lambda_1(\mathbf{q}) = u - a$. Given that $\mathbf{r}_1(\mathbf{q})$ from (71) it is easy to see that Y is a Riemann's invariant for this wave. On the other hand one can also write from (71):

$$\nabla_{\mathbf{q}} w(\mathbf{q}) \cdot \mathbf{r}_1(\mathbf{q}) = -\rho a\left(\frac{\partial w}{\partial p}\right)_u + \left(\frac{\partial w}{\partial u}\right)_p = 0. \tag{80}$$

Hence we get the following second Riemann's invariant:

$$w(p, u) = u + \int_p \frac{\mathrm{d}p}{\rho a}. \tag{81}$$

Hence, to summarize, the Riemann's invariants associated to the 1-wave are given by:

$$\left\{ Y, u + \int_p \frac{\mathrm{d}p}{\rho a} \right\}. \tag{82}$$

When we look at the Riemann's invariants associated to the eigenvalue $\lambda_3(\mathbf{q}) = u + a$ one can show using similar developments that they are given by:

$$\left\{ Y, u - \int_p \frac{\mathrm{d}p}{\rho a} \right\}. \tag{83}$$

Finally, given that $\mathbf{r}_2(\mathbf{q})$ from (71), we get easily the Riemann's invariants associated to the eigenvalue $\lambda_2(\mathbf{q}) = u$:

$$\{u, p\}. \tag{84}$$

3.6. A reduced model in the incompressible liquid limit

In the previous sections, the liquid phase has been considered as a compressible fluid with a small but non-zero compressibility $\mathrm{d}\rho_1/\mathrm{d}p = 1/a_1^2$. However, for almost all practical purposes, one can consider the liquid phase as incompressible with a zero compressibility coefficient. This will lead to a mixture model with a simpler equation of state for the pressure. The purpose of this section is to investigate this limiting case.

Let us introduce the small parameter ϵ defined by $\epsilon = 1/a_1$ and assume that any arbitrary variable ϕ can be expanded in a series in ϵ:

$$\phi = \phi_0 + \epsilon\phi_1 + \mathcal{O}(\epsilon^2). \tag{85}$$

Now, expanding all variables in (20)–(22) and collecting terms having the same power in ϵ, we get the following system for the corresponding power ϵ^0:

$$\frac{\partial \rho}{\partial t} + \nabla \cdot (\rho \mathbf{v}) = 0, \tag{86}$$

$$\frac{\partial \rho \mathbf{v}}{\partial t} + \nabla \cdot (\rho \mathbf{v} \otimes \mathbf{v}) + \nabla p = \rho \mathbf{g}, \tag{87}$$

$$\frac{\partial \rho Y}{\partial t} + \nabla \cdot (\rho Y \mathbf{v}) = -\nabla \cdot (\rho Y (1 - Y) \mathbf{v}_r) \tag{88}$$

with:

$$\mathbf{v}_r = \frac{1}{\lambda} \alpha_1 \alpha_2 \frac{\rho_2 - \rho_1}{\rho} \nabla p, \tag{89}$$

where, for the sake of simplicity, the subscript 0 of the developments (85) has been omitted. Hence, the zero order model is formally equivalent to the fully two-phase compressible original system (20)–(22). On the other hand, the introduction of the expansion (85) in the two equations of state leads for the zero order to:

$$\rho_1 = \rho_L, \tag{90}$$

$$\rho_2 = \frac{p}{a_2^2}. \tag{91}$$

The pressure is thus expressed simply through the relation:

$$p(\rho, \rho Y) = \frac{\rho_L \rho Y a_2^2}{\rho_L - \rho + \rho Y}. \tag{92}$$

This results in a simpler thermodynamic closure. It must also be noticed that in the incompressible liquid limit, the averaged speed of sound is now given by:

$$a^2 = \frac{\rho_2 a_2^2}{\rho \alpha_2}. \tag{93}$$

Fig. 1 compares the sound speed for the compressible model and in the incompressible liquid limit given by (93). It can be seen that for all practical purposes, except in the case of very small gas volume fraction, the two thermodynamical models give identical results.

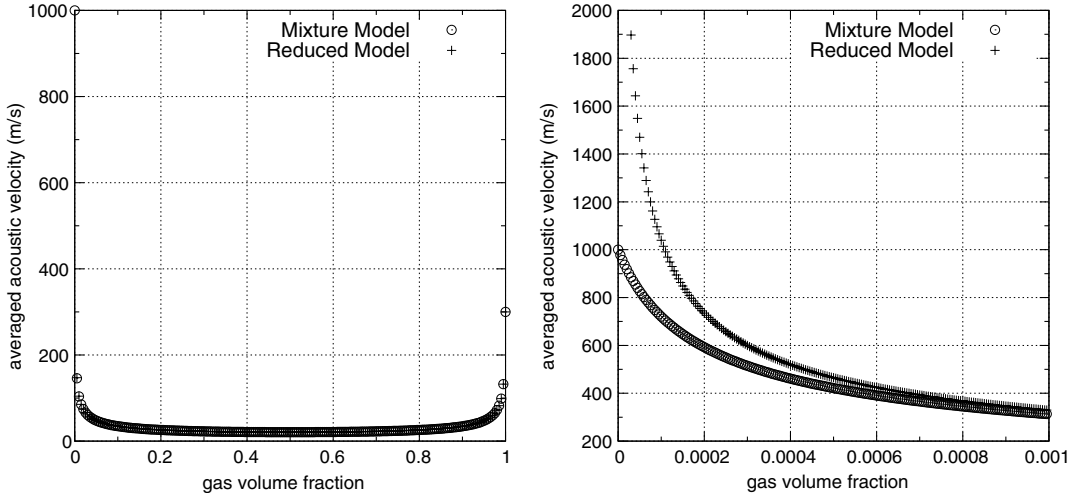

Fig. 1. Mixture sound speed of an air-water system under atmospheric conditions with $a_1 = 1000\ \mathrm{m\ s^{-1}}$ and $a_2 = 300\ \mathrm{m\ s^{-1}}$ for the compressible model (circle) and the model in the incompressible liquid limit (cross). Whole two-phase region (left) and zoom for small gas volume fractions (right).

4. Numerical approximation

The solution is approximated in time by splitting the complete drift-flux mixture model in two steps. The first one corresponds to the convective part which consists in advancing the solution during one time step $\Delta t = t^{n+1} - t^n$ as:

$$\frac{\tilde{\mathbf{Q}}^{n+1} - \mathbf{Q}^n}{\Delta t} + \nabla \cdot \mathscr{F}(\mathbf{Q}^n) = \mathscr{B}(\mathbf{Q}^n) \tag{94}$$

with $\mathscr{F}(\mathbf{Q}) = (\rho u, \rho u^2 + p, \rho Y u)^{\mathrm{t}}$ and $\mathscr{B}(\mathbf{Q}) = (0, -\rho g, 0)^{\mathrm{t}}$. This provides an intermediate solution which is denoted here as $\tilde{\mathbf{Q}}^{n+1}$. Then, the second one corresponds to integrate the second order term in the gas mass fraction conservation equation. In order to avoid a too constrained stability criterion, this step is discretized by a fully implicit scheme which reads:

$$\frac{\mathbf{Q}^{n+1} - \tilde{\mathbf{Q}}^{n+1}}{\Delta t} = -\nabla \cdot \mathscr{D}(\mathbf{Q}^{n+1}, \nabla \mathbf{Q}^{n+1}) \tag{95}$$

with $\mathscr{D}(\mathbf{Q}, \nabla \mathbf{Q}) = (0, 0, \rho Y (1 - Y) \mathbf{v}_r)^{\mathrm{t}}$. The two next sections focuss on the two steps which are approximated in space by means of a finite volume method. In the sequel, these two steps will refer to the convective and the diffusive step respectively.

4.1. Convective step

We present in this section the finite volume scheme corresponding to the first convective step. We adopt the following notation for the cell average at time t^n of the solution on cell K:

$$\mathbf{Q}_K^n = \frac{1}{|K|} \int_K \mathbf{Q}(\mathbf{x}, t^n). \tag{96}$$

Integrating the first step (94) and using the divergence theorem leads to:

$$|K| \frac{\tilde{\mathbf{Q}}_K^{n+1} - \mathbf{Q}_K^n}{\Delta t} + \sum_{\sigma = K|L} |\sigma| \mathbf{\Phi}_\sigma(\mathbf{Q}_K^n, \mathbf{Q}_L^n, \mathbf{n}_\sigma) = |K| \mathscr{B}(\mathbf{Q}_K^n), \tag{97}$$

where $K|L$ denotes the interface between cells K and L and $\mathbf{\Phi}_\sigma$ is the numerical flux at this interface. We have used three different Riemann solvers for estimating the numerical flux. The first corresponds to the Godunov scheme developed in the incompressible liquid limit which consists in calculating the numerical flux as:

$$\mathbf{\Phi}_\sigma(\mathbf{Q}_K^n, \mathbf{Q}_L^n, \mathbf{n}_\sigma) = \mathbf{n}_\sigma \cdot \mathscr{F}(\mathbf{Q}_\sigma^*(\mathbf{Q}_K^n, \mathbf{Q}_L^n)), \tag{98}$$

where $\mathbf{Q}_\sigma^*$ corresponds to the exact Riemann solution at the cell interface σ that corresponds to the characteristic $x_n/t = 0$. A detailed description of the exact solver in the incompressible liquid limit is given in Appendix A. The other two are approximate Riemann solvers and are described in the next two sections.

4.1.1. The VFRoe-ncv scheme

We present in this section an approximate Riemann solver proposed initially by Gallouët and Masella [21] for the Euler equations. We refer to [15,22] for more recent applications of this solver in the frame of two-phase compressible flows. The method consists in replacing the original local Riemann problem at each cell interface by a linearized one and then solve it exactly. Hence, one has to solve at each interface of the mesh the following linearized Riemann problem:

$$\begin{cases} \frac{\partial \mathbf{q}}{\partial t} + \mathbf{A}(\hat{\mathbf{q}}) \frac{\partial \mathbf{q}}{\partial n} = 0, \\ \mathbf{q}(x_n, 0) = \begin{vmatrix} \mathbf{q}_K & \text{if } x_n < 0, \\ \mathbf{q}_L & \text{if } x_n > 0, \end{vmatrix} \end{cases} \tag{99}$$

where x_n denotes the coordinate in the local frame of the interface. The average for estimating the jacobian in (99) corresponds to the arithmetic average between the left and the right states: $\hat{\mathbf{q}} = (\mathbf{q}_K + \mathbf{q}_L)/2$. It is well

known that the properties and then the behavior of this scheme depend on the choice of the variables $\mathbf{q}$. Here, in order to preserve Riemann invariants across contact discontinuities and from numerical experiments performed in [23] the symmetrizing variables $\mathbf{q} = (p, u, Y)^{\mathrm{t}}$ have been selected. Hence, the local jacobian is given by Eq. (69) and the solution of the local linearized Riemann problem at each cell interface is given by:

$$\mathbf{q}^*_\sigma = \mathbf{q}(x_n/t = 0, \mathbf{q}_K, \mathbf{q}_L) = \mathbf{q}_K + \sum_{\hat{\lambda}_k<0} \hat{\alpha}_k \hat{\mathbf{r}}_k = \mathbf{q}_L - \sum_{\hat{\lambda}_k>0} \hat{\alpha}_k \hat{\mathbf{r}}_k, \tag{100}$$

where $\hat{\alpha}_k = \hat{\mathbf{l}}^t_k(\mathbf{q}_L - \mathbf{q}_K)$ and where $\hat{\mathbf{r}}_k$ and $\hat{\mathbf{l}}_k$ are given by (71) and (72) evaluated on $\hat{q}$.

4.1.2. The HLL scheme

We present here the application of the HLL solver [24] to system (20)–(22). This approximate solver offers the advantage to be very simple and is well-known to be very robust while smearing contact discontinuities owing to its two-waves structure description. The HLL-Riemann solver consists of three constant states in the (x_n, t) phase plane, that is:

$$\mathbf{Q}^*_\sigma(x_n/t) = \begin{cases} \mathbf{Q}_K & \text{if } x_n/t < S_K, \\ \mathbf{Q}_{hll} & \text{if } S_K \leqslant x_n/t \leqslant S_L, \\ \mathbf{Q}_L & \text{if } x_n/t > S_L, \end{cases} \tag{101}$$

where S_K and S_L correspond, respectively, to the smallest and the largest wave speeds. The numerical flux function corresponding to the intermediate state is given by:

$$\mathbf{\Phi}^{hll}_\sigma = \frac{S_L \mathscr{F}(\mathbf{Q}_K) - S_K \mathscr{F}(\mathbf{Q}_L) + S_K S_L (\mathbf{Q}_L - \mathbf{Q}_K)}{S_L - S_K}. \tag{102}$$

Then, the complete intercell numerical flux is given by:

$$\mathbf{\Phi}_\sigma = \begin{cases} \mathscr{F}(\mathbf{Q}_K) & \text{if } 0 < S_K, \\ \mathbf{\Phi}^{hll}_\sigma & \text{if } S_K \leqslant 0 \leqslant S_L, \\ \mathscr{F}(\mathbf{Q}_L) & \text{if } 0 > S_L. \end{cases} \tag{103}$$

At this point, it remains to provide estimates for the wave speeds S_K and S_L. We use here the standard estimate:

$$S_K = \min(u_K - a_K, u_L - a_L), \quad S_L = \max(u_K + a_K, u_L + a_L). \tag{104}$$

4.2. Diffusive step

The discretisation of the diffusive step takes advantages of the particular form of the gas mass fraction equation that writes

$$\frac{\partial \rho Y}{\partial t} + \nabla \cdot (\rho \mathbf{v} Y) = -\nabla \cdot (f(Y) \rho \mathbf{v}_r) \tag{105}$$

with $f(Y) = Y(1 - Y)$. Integration of (95) on a cell K and applying the divergence theorem leads to:

$$|K| \rho^{n+1} \frac{Y^{n+1}_K - \tilde{Y}^{n+1}_K}{\Delta t} + \sum_{\sigma=K|L} |\sigma| [f_\sigma(Y_K, Y_L)(\mathbf{n} \cdot \rho \mathbf{v}_r)^+_\sigma + f_\sigma(Y_L, Y_K)(\mathbf{n} \cdot \rho \mathbf{v}_r)^-_\sigma]^{n+1} = 0, \tag{106}$$

where we have already used $\rho^{n+1} = \tilde{\rho}^{n+1}$. In (106) we have introduced the standard notation $\mathbf{v}^\pm_r = (\mathbf{v}_r \pm |\mathbf{v}_r|)/2$. The function $f_\sigma(Y_K, Y_L)$ corresponds to a monotone flux discretization of $f(Y) = Y(1 - Y)$ which satisfies the following properties [25]:

- f_σ is locally Lipschitz continuous from $\mathbb{R}^2$ to $\mathbb{R}$,
- $f_\sigma(Y, Y) = f(Y)$ for all $Y \in [Y_K, Y_L]$,

– $(a,b) \to f_\sigma(a,b)$, from $Y \in [Y_K, Y_L]^2$ to $\mathbb{R}$, is non-decreasing with respect to a and non-increasing with respect to b.

Several choices are possible for the numerical flux function f_σ and we refer to Eymard et al. [25] for some examples and cited references. We adopt here the following simple flux-splitting formula:

$$f_\sigma(a,b) = f_{1\sigma}(a) + f_{2\sigma}(b), \tag{107}$$

where $f_{1\sigma}(a) = a$ and $f_{2\sigma}(b) = -b^2$ are, respectively, non-decreasing and non-increasing functions. Such a monotone flux discretization ensures the existence and the unicity of the solution of (106) together with the fact that this solution lies in the physical interval $[0,1]$ [26].

On the other hand, we use the following approximation for estimating $(\mathbf{n}\cdot\rho\mathbf{v}_r)_\sigma$ at each cell interface:

$$(\mathbf{n}\cdot\rho\mathbf{v}_r)_\sigma^{n+1} = \rho_\sigma^{n+1}\frac{Y_\sigma^{n+1} - \tilde{\alpha}_\sigma^{n+1}}{\lambda}\frac{p_K^{n+1} - p_L^{n+1}}{d_\sigma}\frac{\mathbf{d}_\sigma\cdot\mathbf{n}_\sigma}{d_\sigma} \tag{108}$$

with $\phi_\sigma = (\phi_K + \phi_L)/2$ for $\phi = \rho, Y, \alpha$ and $\mathbf{d}_\sigma$ is the oriented vector from node K to node L with d_σ the corresponding measure. In Eq. (108), the notation p^{n+1} refers to $p(\rho^{n+1}, Y^{n+1})$ where we recall that ρ^{n+1} corresponds to the solution given by the first convective step. A Newton algorithm is used to solve Eq. (106). In practice, only three iterations are necessary to reach convergence.

5. Numerical results

5.1. Moving contact discontinuity

The first test case is a standard test case for simulating multiphase materials and consists in the advection of a material interface between air and water. Initial data correspond to a material interface located at $x = 0$ in a tube of length $L = 1$ m with water on the left and air on the right. The density of the two phases are $\rho_1 = 1000\ \mathrm{kg\,m^{-3}}$ and $\rho_2 = 1.2\ \mathrm{kg\,m^{-3}}$ for water and air respectively. Both the pressure and the velocity are initially constant: $p = 10^5$ Pa and $u = 1000\ \mathrm{m\,s^{-1}}$. The averaged sound velocity being infinite for a purely liquid mixture, the void fraction is set to $\alpha_2 = 10^{-3}$ on the left of the material interface while $\alpha_2 = 1$ on the right.

The tube is discretized with 1000 cells, the time scheme is explicit with a CFL number equal to 0.4. The results are shown at time $t = 210^{-4}$ s in Fig. 2 using the Godunov (dashed line), the VFRoe-ncv (circle) and the HLL (cross) solvers. These three solvers exactly preserve both constant velocity and pressure across the contact discontinuity. The analytical proof of this result is given in Appendix B.

5.2. Stationary shock

We show through this test case that the mixture Darcy drift model presents an interesting and rather unusual property. Namely that the presence of the drift terms prevents the mass fraction to being constant inside a shock.

In a first step, we assume that the drift (or relative) velocity is zero, then the Rankine–Hugoniot relations for the system (20)–(22) are:

$$\Delta[\rho u] = u_s\Delta[\rho], \tag{109}$$

$$\Delta[\rho Y u] = u_s\Delta[\rho Y], \tag{110}$$

$$\Delta[\rho u^2 + p] = u_s\Delta[\rho u], \tag{111}$$

where u_s denotes the shock velocity. Combining the first equation (109) and the second one (110), one can check that if the mass flux $\rho(u - u_s)$ across the discontinuity is non-zero, then the mass fraction Y is constant across the discontinuity. We test this result considering a stationary discontinuity located at $x = 0$ m in a tube of length $L = 1.2$ m between the following two states:

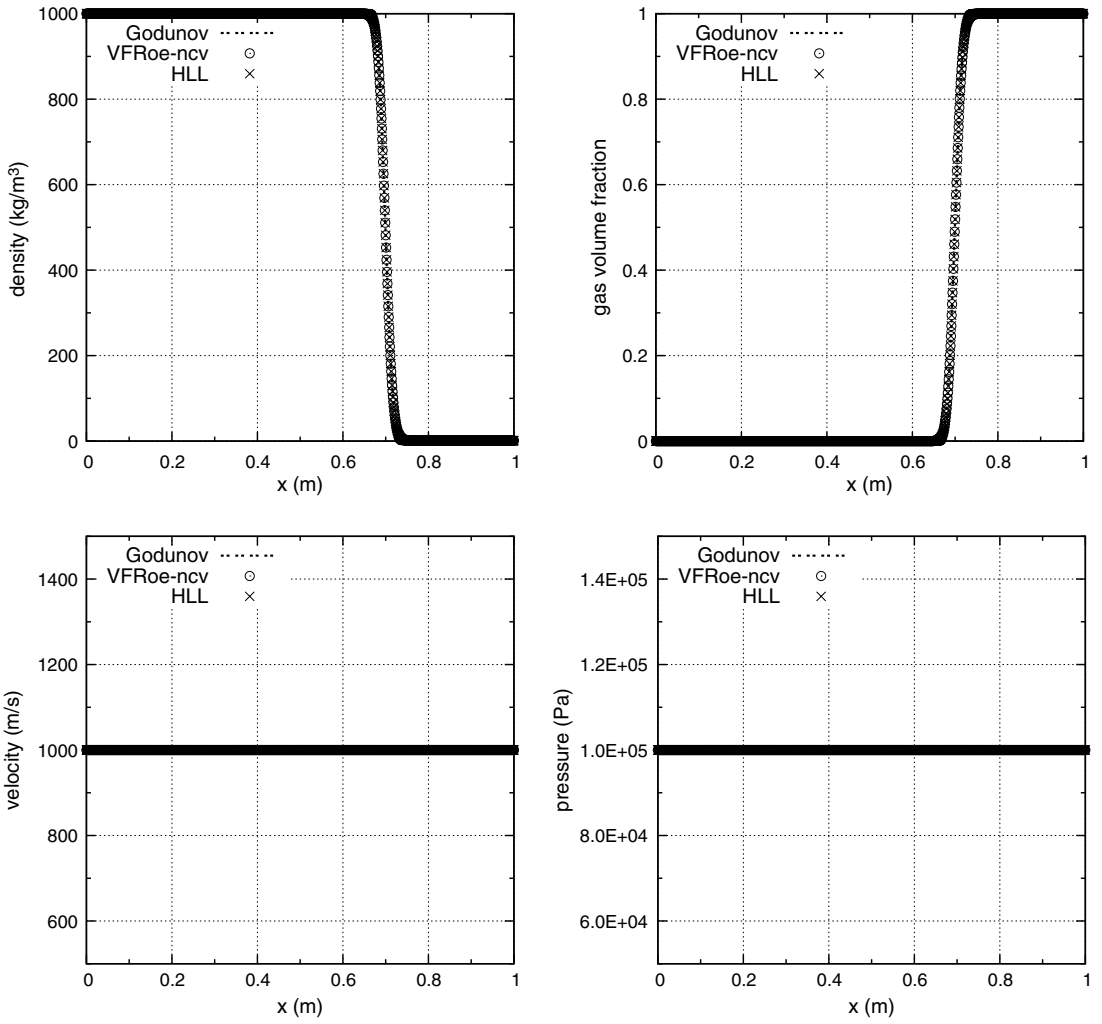

Fig. 2. Moving contact discontinuity.

$$\begin{pmatrix} \rho_2 \\ u \\ Y \end{pmatrix}_L = \begin{pmatrix} 0.099 \\ 10. \\ 10^{-4} \end{pmatrix}, \quad \begin{pmatrix} \rho_2 \\ u \\ Y \end{pmatrix}_R = \begin{pmatrix} 0.2973 \\ 10. - 3.3519693 \\ 10^{-4} \end{pmatrix}.$$

As shown in Fig. 3 one can check that the Godunov scheme is able to compute the exact solution for this case and to capture the discontinuity on one point.

We now perform the same computation using the Darcy drift law (23). Here, we simply take a constant value of the drag coefficient λ and we adopt the standard procedure of [27,28] to estimate this value. This technique consists in setting first $\lambda = \alpha_2 C_w$ and then neglecting all terms in the gas momentum equation except the drag force and the pressure gradient. This leads to:

$$\mathbf{v}_r = -\frac{\nabla p}{C_w}. \tag{112}$$

This relation allows to relate directly the coefficient C_w to the terminal velocity of a rising bubble in the case of non-interacting single bubbles in a stagnant liquid. For instance, the commonly adopted value of the velocity of a single air bubble rising in water is about 0.2 m.s^{-1}. This corresponds roughly to $C_w = 5.10^4$ kg m^{-3} s^{-1} for α_2 around 0.5. In the numerical experiment reported here, we have used the constant value $\lambda = 10^4$ kg m^{-3} s^{-1}

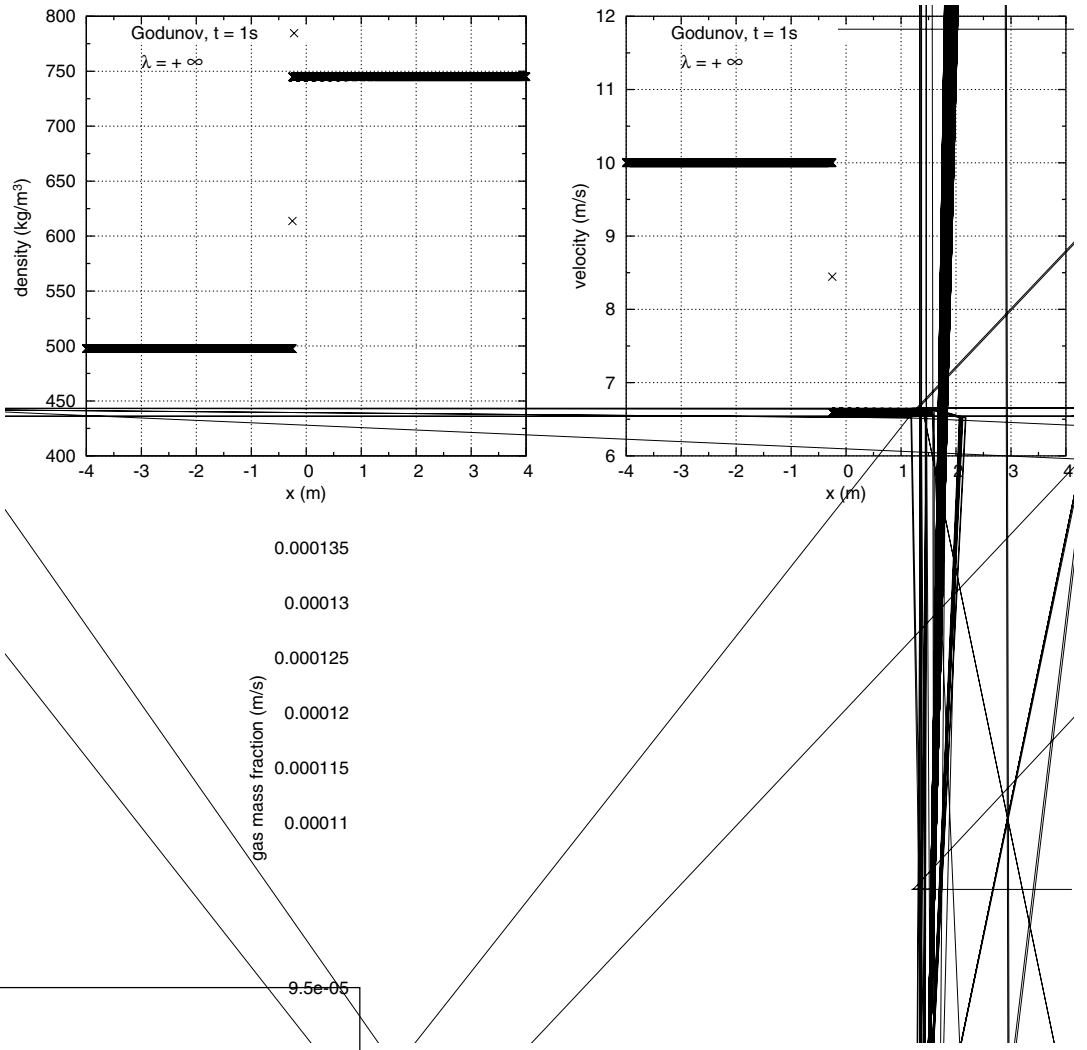

that corresponds to the same order of magnitude. For the test-case reported here, the use of different values of λ does not change the structure of the solution but simply modify the thickness of the shock zone. The results are displayed in Fig. 4. In order to capture the shock zone, we use a refined mesh with 4000 nodes and compute the solution until a steady state is obtained. One can check that the mass fraction is not constant inside the shock zone and this contrasts to the previous case. Indeed, consider a travelling wave of speed u_s separating two constant states $(\rho_2, u, Y)_L$ and $(\rho_2, u, Y)_R$ in $x = -\infty$ and $x = +\infty$. Integration of the first two equations of the system (20)–(23) between $-\infty$ and x leads to:

$$\rho(x)[u(x) - u_s] = \rho_L[u_L - u_s], \tag{113}$$

$$\rho(x)Y(x)[u(x) + (1 - Y(x))u_r(x) - u_s] = \rho_L Y_L[u_L - u_s], \tag{114}$$

where we have used that in $x = -\infty$ the drift velocity u_r (proportional to the pressure gradient) is zero. Hence, introducing the mass flux $m_L = \rho_L[u_L - u_s]$, combination of these two equations leads to:

$$m_L[Y(x) - Y_L] = -\rho(x)Y(x)(1 - Y(x))u_r(x) = -Y(x)(1 - Y(x))\alpha_1(x)\alpha_2(x)(\rho_2(x) - \rho_1(x))\frac{\partial p}{\partial x}. \tag{115}$$

If $m_L > 0$ and since in a right propagating shock, the pressure gradient is positive, this leads to:

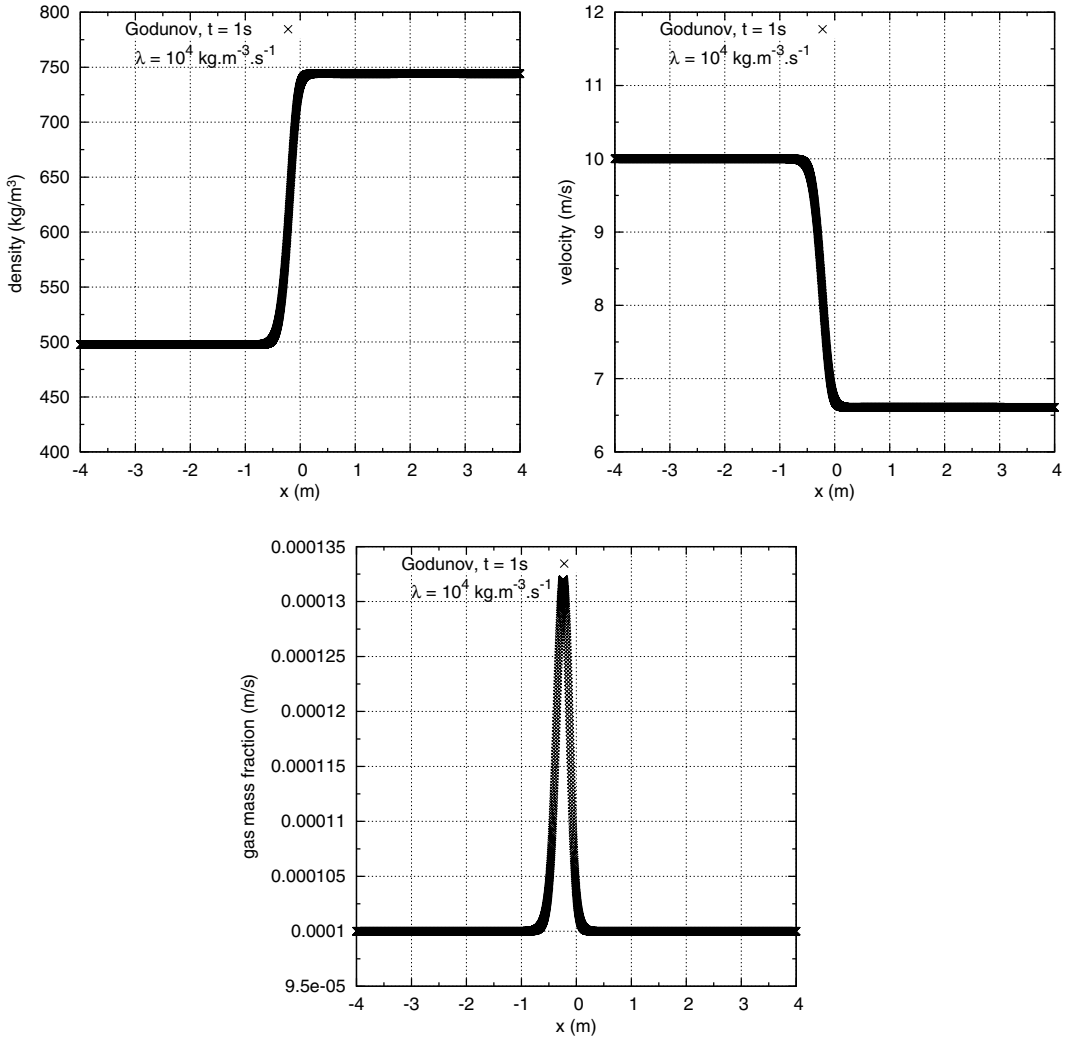

Fig. 4. Stationary shock, finite drag coefficient $\lambda = 10^4\ \mathrm{kg\,m^{-3}\,s^{-1}}$.

$$Y(x) \geqslant Y_L. \tag{116}$$

That is exactly what can be noticed from the numerical experiment in Fig. 4. This behavior is in clear contrast with the behavior of multicomponent models where the drift velocity is modeled by a Fick law.

5.3. Two-fluid shock tube

We present here numerical results for the two-fluid shock tube problem presented in [13] with a slip hydrodynamic law. The computation is performed in a tube of length $L = 100$ m with a discontinuity between the two initial constant states located at $x = 50$ m. For this test case, the gas sound speed is fixed to: $a_2 = 300\ \mathrm{m\,s^{-1}}$. The two states are given by:

$$\begin{pmatrix} \rho \\ u \\ Y \end{pmatrix}_L = \begin{pmatrix} 453.197 \\ 24.8074 \\ 0.00705 \end{pmatrix}, \quad \begin{pmatrix} \rho \\ u \\ Y \end{pmatrix}_R = \begin{pmatrix} 454.915 \\ 1.7461 \\ 0.0108 \end{pmatrix}.$$

The hydrodynamic law used in [13] corresponds to the Zuber–Findlay [29] correlation which can be written as:

$$u_r = \frac{u_\infty - (1 - c_0)u}{1 - \alpha_2 c_0 - Y(1 - c_0)}, \tag{117}$$

where c_0 is the so-called distribution parameter and u_∞ the terminal velocity of a single bubble in a quiescent liquid. In [13], the values $u_\infty = 0.2162$ m/s and $c_0 = 1.07$ have been used. To compare our model with such a highly empirical relation for the relative velocity, we investigate this case by following the procedure described in the previous numerical experiment and set here directly the value: $\lambda = C_w = 5.10^4$ kg m^{-3} s^{-1} that corresponds roughly to the same terminal velocity.

Numerical results are presented in Fig. 5 at time $t = 0.5$ s using the Godunov, VFRoe-ncv and HLL solvers with 5000 nodes using an explicit time integration for the first convective step and a constant CFL number equal to 0.5. The results are globally identical for the three schemes except that the Godunov and VFRoe solver produce small oscillations on the solution for the density and the gas mass fraction located near the contact discontinuity. These small oscillations are not present when using the more diffusive HLL solver. These small oscillations disappear when using smaller values of the coefficient λ and therefore can be due to a lack of spacial resolution.

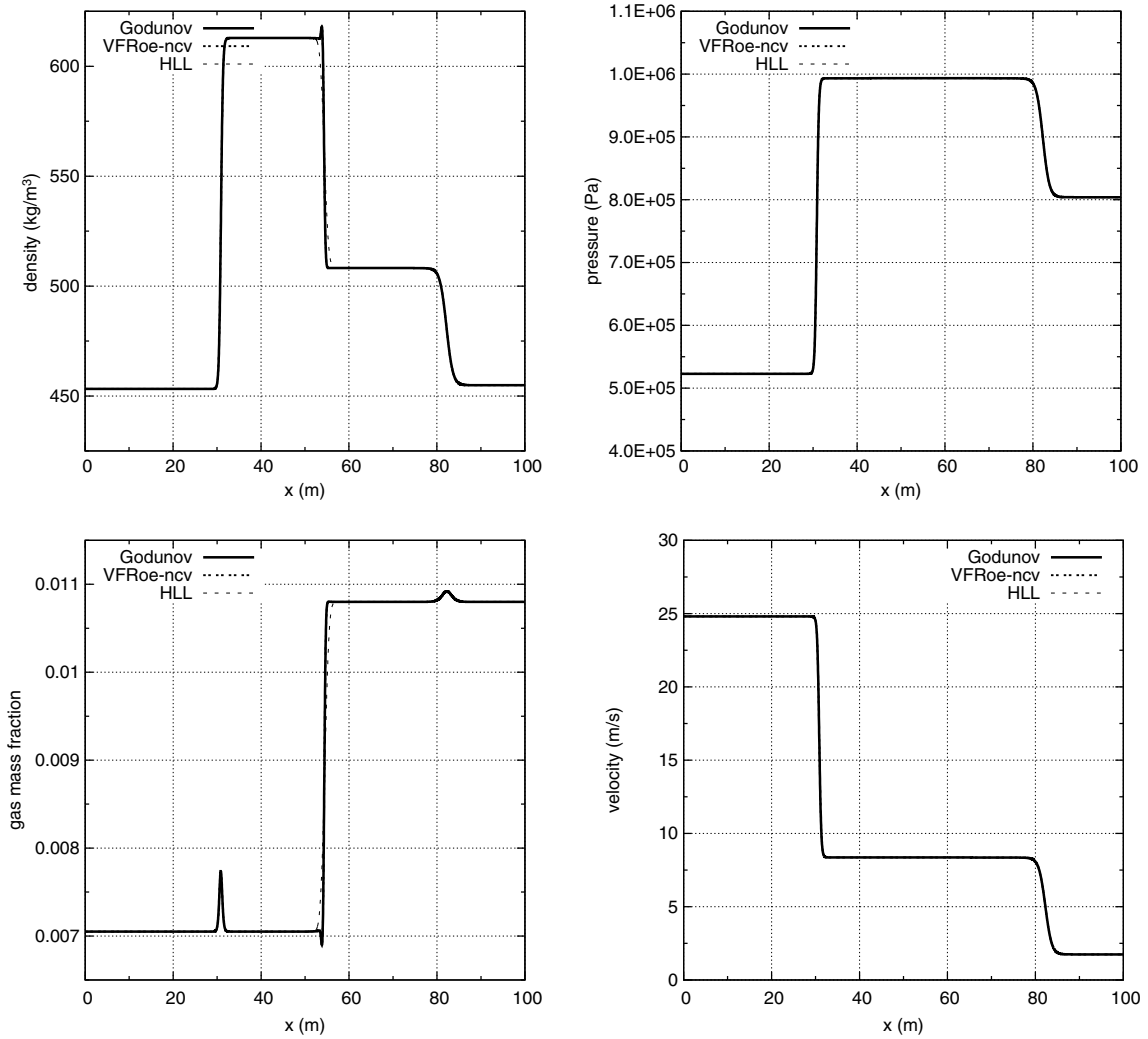

Fig. 5. Two fluid shock tube problem with drag: shock-contact discontinuity-shock pattern. Results obtained with $\lambda = 5 \times 10^4$ kg m^{-3} s^{-1}.

The results are surprisingly close to those obtained in [13] given the very different nature of the two models used. The general structure of the solution that corresponds to a shock-contact discontinuity-shock pattern is the same and the same wave speeds are observed. The main difference occurs on the gas mass fraction. In the Drift-flux model of [13], the passage of the shock creates a plateau with higher values of the gas mass fraction while for the Darcy drift model, the gas mass fraction returns to its initial value after the passage of the shocks.

5.4. Water faucet problem

We continue this presentation of numerical test cases by two problems for which a priori the Darcy drift mixture model is inappropriate. These problems involve the decoupling of the motion of the liquid and gas and should require the use of two-fluid models. The first problem is the water faucet problem, a very standard test case for simulating two-phase flows using a two-fluid model [5,30,31].

This test consists in a vertical tube of length $L = 12$ m initially filled with a two-phase mixture of air and water with $\alpha_2 = 0.2$. The velocity of the water u_1 is initially equal to 10 m s^{-1} while the velocity of the air u_2 is null. For $t > 0$, the gravity field is introduced $g = 9.81$ m^2 s^{-1} and the boundary conditions correspond to a

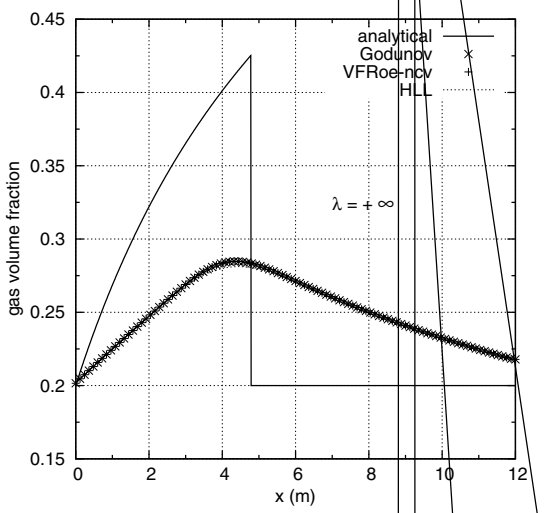

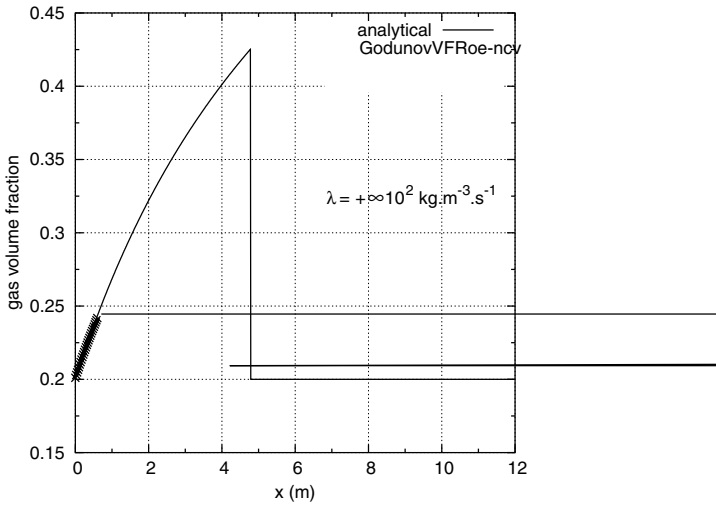

Godunov

flow of water at the top boundary with $u_1 = 10\ \mathrm{m\ s^{-1}}$, $u_2 = 0\ \mathrm{m\ s^{-1}}$ and $\alpha_2 = 0.2$, while the bottom boundary corresponds to an outflow condition with the prescribed constant pressure $p = 10^5$ Pa.

The simulation of the water faucet problem is usually performed with a null drag force. Under the assumption of a constant pressure in the gaseous phase, the problem admits an analytical solution for the void fraction (e.g. [32]):

$$\alpha_2 = \begin{cases} 1 - \dfrac{(1-\alpha_2^0)u_1^0}{\sqrt{2gx + (u_1^0)^2}} & \text{if } x \leqslant u_1^0 t + \dfrac{gt^2}{2}, \\ 0.2 & \text{otherwise,} \end{cases} \tag{118}$$

where α_2^0 and u_1^0 correspond, respectively, to the initial void fraction and water velocity. In our numerical simulation, the inflow state is computed here using Riemann's invariants across the outgoing characteristic λ_1. In the case of the reduced model in the incompressible liquid limit, the Riemann invariants given by (82) simplify to:

$$Y_e = Y_i, \tag{119}$$

$$u_e + a_2\sqrt{Y_e}\ln\frac{\rho_{2e}}{\rho_1 Y_e} = u_i + a_2\sqrt{Y_i}\ln\frac{\rho_{2i}}{\rho_1 Y_i}, \tag{120}$$

where the subscript e refers to the inflow state while the subscript i denotes the cell values adjacent to the boundary. From these invariants, one can write the following relation for the inflow density:

$$a_2\sqrt{1 - \frac{1-\alpha_{2e}}{\rho_e}\rho_1}\ln\frac{\rho_e\alpha_{2i}}{\rho_i\alpha_{2e}} + u_e - u_i = 0. \tag{121}$$

Hence, given the prescribed velocity u_e and void fraction α_{2e} at the inflow boundary, the inflow density is computed from Eq. (121) using an iterative algorithm.

The numerical results are shown in Fig. 6 using +500 nodes and a constant CFL number equal to 0.4. It can be checked that for $\lambda = +\infty$ that is for a relative velocity equal to zero, the solution given by the Darcy drift model (that reduces in this case to an homogeneous model) is totally false. However, for small values of the drag coefficient: $\lambda = 10^2$ and $10^{-2}\ \mathrm{kg\ m^{-3}\ s^{-1}}$, the solution becomes in good agreement with the analytical solution and of comparable accuracy with solutions obtained with two-fluid models. Moreover, as seen in Fig. 7, that displays the results of a mesh convergence study using the Godunov scheme, the numerical solution converge to the analytical solution. These results seem to indicate that the domain of validity of the Darcy drift model is not limited to large values of the velocity relaxation parameter.

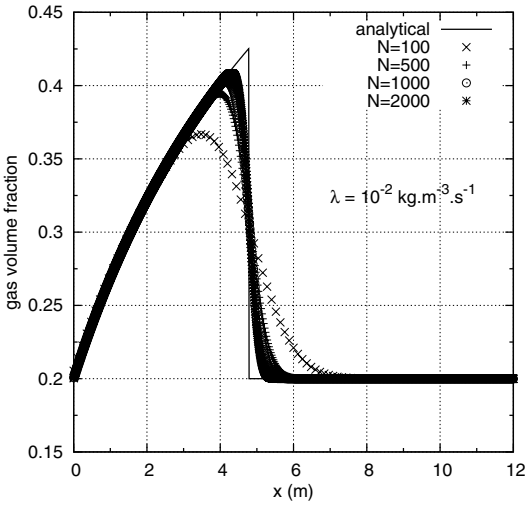

Fig. 7. Ransom's water faucet problem; Results at time $t = 0.4$ s for $\lambda = 10^{-2}\ \mathrm{kg\ m^{-3}\ s^{-1}}$; Mesh convergence study using the Godunov scheme.

5.5. Sedimentation

Our last test problem also involves a decoupling of the motion of the liquid and the gas which requires the use of a two-fluid model. Hence, for this problem, it is also expected that the Darcy drift model is a priori inadequate for simulating this problem.

We present here numerical results obtained with the proposed Darcy drift model for the sedimentation test problem. This problem is also a classical benchmark test for the two-fluid models [22,30–32].

We consider a vertical tube of length $L = 7.5$ m filled with a two-phase mixture of air and water with $\rho_1 = 1000\ \mathrm{kg\,m^{-3}}$ and $\rho_2 = 1.2\ \mathrm{kg\,m^{-3}}$ at the ambient pressure $p_0 = 10^5$ Pa. Initial conditions correspond to $\alpha_2 = 0.5$, $u = 0\ \mathrm{m\,s^{-1}}$ and $p = p_0$. The domain is closed and thus both the top and the bottom boundaries correspond to reflective conditions.

Then, at time $t = 0$ s, the two-phase mixture is set under the action of the gravity $g = 9.81\ \mathrm{m\,s^{-2}}$ which provides phase separation for $t > 0$. In the frame of the two-fluid models, this test is usually performed neglecting all forces, including the interfacial drag force, excepted the gravity.

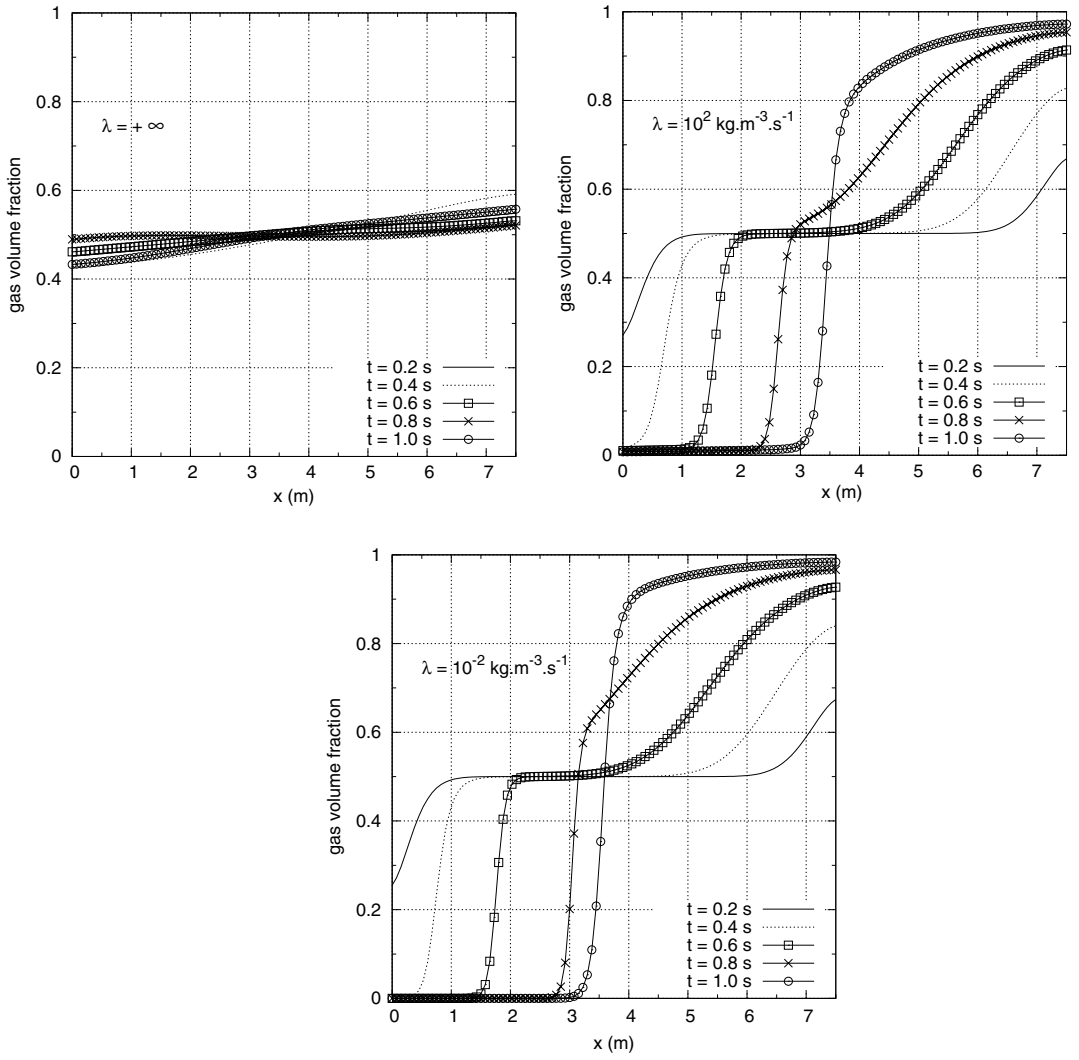

Fig. 8. Variation of the gas volume fraction α_2 for the sedimentation problem for $\lambda = +\infty$ (homogeneous model), $\lambda = 10^2\ \mathrm{kg\,m^{-3}\,s^{-1}}$ and $\lambda = 10^{-2}\ \mathrm{kg\,m^{-3}\,s^{-1}}$.

Here we mimic these conditions by investigating two different values for the velocity relaxation coefficient: $\lambda = 10^2$ and 10^{-2} kg m^{-3} s^{-1}. We have also included the solution corresponding to the homogeneous mixture model which is obtained in the limit $\lambda = +\infty$.

The results displayed in Fig. 8 show clearly that the homogeneous mixture model corresponding to $\lambda = +\infty$ does not reproduce the separation phenomenon. On the other hand, the solution obtained with smaller values for the coefficient λ are in good agreement with well-known solutions produced by two-fluid models. This is quite surprising and constitutes to the best of our knowledge an original result obtained with such a simple model.

From the computational point of view, we also note that this computation is difficult for the present explicit numerical scheme used in the convective step. Actually, as separation occurs, α_2 becomes small in the liquid part of the domain and then according to (93) (see Fig. 1), the speed of sound rises to infinity and the computed time step becomes extremely small as the (quasi) liquid region develops. It is therefore extremely difficult to advance in time with the present explicit method. In addition, we have also noted that the VFRoe solver produces negative values for the gas mass fraction in the cell adjacent to the wall boundary in the liquid region. Therefore, the computations reported here have been performed only with the HLL solver using 100 cells and a constant CFL number equal to 0.4. Due to the quite diffusive nature of this solver, even if separation occurs, the value of the gas volume fraction in the quasi-liquid region are not too small and the solution can be advanced in time at a reasonable cost.

6. Conclusion

In two-phase flows, except for very simple or specialized cases, the velocities of the two phases are usually different. For this reason, two phase flow modeling is usually performed either by two-fluid models with two velocities and one pressure or by simpler drift-flux models where the difference of the velocities of the two phases is given by algebraic correlations. In the two cases, this leads to serious mathematical and numerical difficulties. The first-order part of these models is usually not hyperbolic and therefore one has to rely on second-order diffusive terms to insure the well-posedness of the models. Moreover, from the numerical point of view, one has to give up the standard approximation methods and devise appropriate numerical schemes with unknown convergence properties.

Here, we have proposed to investigate another type of models where the relative velocity between the phases is given by a Darcy law. We have shown that this relation appears naturally in a Chapman–Enskog first-order asymptotic approximation of the two-fluid models. The convective part of the model is always hyperbolic and standard approximation methods can be used for its discretization. Moreover, the second-order part of the model given by the Darcy law is dissipative and its particular structure allows to use a numerical scheme that preserves the maximum principle. The applications of the model to some standard problems in two-phase modeling are particularly satisfactory given the simplicity of the model.

Acknowledgments

Part of this study has been done during the Ph.D. Thesis of Roxanna Panescu [23]. The authors are also pleased to acknowledge the support of Jean-Claude Latché of IRSN during this work.

Appendix A. Godunov solver in the incompressible liquid limit

In this section, we give a quick description of the exact Godunov solver used to compute approximate solutions of the system

$$\frac{\partial \rho}{\partial t} + \frac{\partial \rho u}{\partial x} = 0, \tag{A.1}$$

$$\frac{\partial \rho u}{\partial t} + \frac{\partial (u^2 + p)}{\partial x} = 0, \tag{A.2}$$

$$\frac{\partial \rho Y}{\partial t} + \frac{\partial \rho Y u}{\partial x} = 0 \tag{A.3}$$

with the state law:

$$p(\rho,\rho Y)=\rho_2 a_2^2=\frac{\rho_L \rho Y a_2^2}{\rho_L-\rho+\rho Y}. \tag{A.4}$$

The Godunov flux being given by

$$\mathbf{\Phi}(\mathbf{Q}_L^n,\mathbf{Q}_R^n)=\mathscr{F}(\mathbf{Q}^*(\mathbf{Q}_L^n,\mathbf{Q}_R^n)), \tag{A.5}$$

where $\mathbf{Q}^*$ corresponds to the exact Riemann solution at the cell interface, the description of the solver reduces to the computation of this interface value. First, we note that due to the eigenstructure of the system given in Section 3.4, the solution of the Riemann problem will be composed of four states separated by a 1-wave associated with the genuinely nonlinear field $\lambda_1(\mathbf{Q})=u-a$, a contact discontinuity associated with the linearly degenerate field $\lambda_2(\mathbf{Q})=u$ and a 3-wave associated with the genuinely nonlinear field $\lambda_3(\mathbf{Q})=u+a$. Across the 2-wave, pressure and velocity are constant by the relation (84). Let us denote, p^*,u^*, the values of these variables across this wave. We note that due to the state law $p=\rho_2 a_2^2$ where a_2 is the (constant) speed of sound in the gas phase, it is equivalent to find the value of the couple ρ_2^*,u^* and we will use these variables in the sequel. Now, since, Y is constant across a shock wave and by (82), (83) is also constant across 1-rarefaction and 3-rarefaction waves, we will have

$$Y(x/t)=\begin{cases} Y_L & \text{if } x/t<u^*,\\ Y_R & \text{else}\end{cases} \tag{A.6}$$

and thus, the problem reduces to find the value of the couple ρ_2^*,u^*.

Let us denote $\mathscr{C}_3(\rho_2)$ the curve in the ρ_2,u plane defining the states ρ_2,u that can be connected to a given right state ρ_2^R,u^R either by a 3-shock or by a 3-rarefaction wave. Using the Rankine–Hugoniot relations (109)–(111) as well as the expression of the Riemann invariants (83) one obtains:

$$u=\mathscr{C}_3(\rho_2)\begin{cases} u^R+\sqrt{a_2^2Y^R}\frac{\rho_2-\rho_2^R}{\sqrt{\rho_2\rho_2^R}} & \text{if } \rho_2>\rho_2^R,\\ u^R-\sqrt{a_2^2Y^R}Ln\frac{\rho_2^R}{\rho_2} & \text{else.}\end{cases} \tag{A.7}$$

Similarly, if we note $\mathscr{C}_1(\rho_2)$ the curve in the ρ_2,u plane defining the states ρ_2,u that can be connected to a given left state ρ_2^L,u^L either by a 1-shock or by a 1-rarefaction wave, use of the Rankine–Hugoniot relationships and of the expression of the Riemann invariants (82) will give us

$$u=\mathscr{C}_1(\rho_2)\begin{cases} u^L-\sqrt{a_2^2Y^L}\frac{\rho_2-\rho_2^L}{\sqrt{\rho_2\rho_2^L}} & \text{if } \rho_2>\rho_2^L,\\ u^L+\sqrt{a_2^2Y^L}Ln\frac{\rho_2^L}{\rho_2} & \text{else.}\end{cases} \tag{A.8}$$

The expression of ρ_2^*,u^* is then obtained by computing the intersection of these two curves. One can note that since $\rho_2=0$ is an asymptote to the curves $\mathscr{C}_1(\rho_2)$ and $\mathscr{C}_3(\rho_2)$, the intersection of these two curves always exists and is unique.

Appendix B. Numerical preservation of velocity and pressure through a contact discontinuity

The key argument of the proofs lies in the linearity of ρY with ρ at fixed p in the equation of state. Using similar developments as those used by Gallouët et al. [33] and Murrone and Guillard [15], we show here that any Godunov solver preserving both the velocity and the pressure for the intermediate state also preserves the cell values of the velocity and the pressure for the barotropic Darcy drift model in the incompressible liquid limit. This is obviously the case for the exact Godunov solver presented in the previous section and this is also the case for the VFRoe-ncv solver using primitive variables $(p,u,Y)^{\mathrm{t}}$ as demonstrated in [33].

Let us note $\lambda=\Delta t/\Delta x$, the starting point consists in writing the discrete version of the mass conservation equation for the ith cell using the known intermediate state $u_{i\pm1/2}^n=u_0$:

$$\rho_i^{n+1}=\rho_i^n-\lambda((\rho u)_{i+1/2}^n-(\rho u)_{i-1/2}^n)=\rho_i^n-\lambda u_0(\rho_{i+1/2}^n-\rho_{i-1/2}^n). \tag{B.1}$$

In the same way, using the known intermediate state $p^n_{i\pm1/2} = p_0$, the discrete form of the momentum conservation equation writes:

$$\begin{aligned}(\rho u)_i^{n+1} &= (\rho u)_i^n - \lambda((\rho u^2 + p)^n_{i+1/2} - (\rho u^2 + p)^n_{i-1/2}) = (\rho u)_i^n - \lambda((\rho^n_{i+1/2} u_0^2 + p_0) - (\rho^n_{i-1/2} u_0^2 + p_0)) \\ &= \rho_i^n u_0 - \lambda u_0^2(\rho^n_{i+1/2} - \rho^n_{i-1/2}). \end{aligned} \tag{B.2}$$

Hence, by using the mass conservation Eq. (B.1), this show that $u_i^{n+1} = u_0$.

At this point, the preservation of the pressure remains to be studied through the gas mass fraction conservation equation. Using the same notations, the discrete finite volume version of the gas mass fraction equation writes:

$$(\rho Y)_i^{n+1} = (\rho Y)_i^n - \lambda[(\rho u Y)^n_{i+1/2} - (\rho u Y)^n_{i-1/2}] = (\rho Y)_i^n - \lambda u_0[(\rho Y)^n_{i+1/2} - (\rho Y)^n_{i-1/2}]. \tag{B.3}$$

Then, from Eq. (92)

References

[1] D. Drew, Mathematical modeling of two-phase flow, Annu. Rev. Fluid Mech. 15 (1983) 261–291.
[2] M. Ishii, Thermo-fluid dynamic theory of two-phase flow, Collection de la Direction des Etudes et Recherches d'Electricité de France, Eyrolles, Paris, 1975.
[3] H.B. Stewart, B. Wendroff, Two-phase flow: models and methods, J. Comput. Phys. 56 (1984) 363–409 (review article).
[4] M. Baer, J. Nunziato, A two-phase mixture theory for the deflagration-to-detonation transition (DDT) in reactive granular materials, Int. J. Multiphase Flow 12 (1986) 861–889.
[5] R. Saurel, R. Abgrall, A multiphase Godunov method for compressible multifluid and multiphase flows, J. Comput. Phys. 150 (1999) 425–467.
[6] J. Cortes, A. Debussche, I. Toumi, A density perturbation method to study the eigenstructure of two-phase flow equation systems, J. Comput. Phys. 147 (1998) 463–484.
[7] D. Bestion, The physical closure laws in the CATHARE code, Nucl. Eng. Des. 124 (1990) 229–245.
[8] R. Lahey, The prediction of phase distribution and separation phenomena using two-fluid models, Boiling Heat Transfer (1992) 85–121.
[9] I. Toumi, An upwind numerical method for a 6 equations two-phase flow model, Nucl. Eng. Des. 123 (1996) 147–168.
[10] G.B. Wallis, One-Dimensional Two-Phase Flow, McGraw-Hill, New York, 1969.
[11] S. Benzoni-Gavage, Analyse numérique des modèles hydrodynamique d'écoulements diphasiques instationnaires dans le s réseaux de production pétrolières, Ph.D. Thesis, Ecole Normale Supérieure de Lyon, 1991.
[12] I. Faille, E. Heintzé, A rough finite volume scheme for modeling two-phase flow in a pipeline, Comput. Fluids 28 (1999) 213–241.
[13] M. Baudin, C. Berthon, F. Coquel, R. Masson, Q. Tran, A relaxation method for two-phase flow models with hydrodynamic closure law, Numer. Math. 99 (2005) 411–440.
[14] S. Clerc, Numerical simulation of the homogeneous equilibrium model for two-phase flows, J. Comput. Phys. 161 (2000) 354–375.
[15] A. Murrone, H. Guillard, A five equation reduced model for compressible two phase flow problems, J. Comput. Phys. 202 (2) (2005) 664–698.
[16] A. Kapila, R. Menikoff, J. Bdzil, S. Son, D. Stewart, Two-phase modeling of deflagration-to-detonation transition in granular materials: reduced equations, Phys. Fluids 13 (10) (2001) 3002–3024.
[17] M. Ishii, N. Zuber, Drag coefficient and relative velocity in bubbly, droplet or particulate flows, AIChE J. 25 (5) (1979) 843–855.
[18] M. Ishii, K. Mishima, Two-fluid model and hydrodynamic constitutive relations, Nucl. Eng. Des. 82 (1984) 107–126.
[19] G. Chen, C. Levermore, T. Liu, Hyperbolic conservation laws with stiff relaxation terms and entropy, Comm. Pure Appl. Math. 47 (1994) 787–830.
[20] B. Michel, Physical models and governing equations for a multiphase multispecies solidifying flow spreading on an abatable substrate, Technical Report IRSN/DRS/SEMAR-02-57, IRSN, 2002.
[21] T. Gallouët, J. Masella, Un schéma de godunov approché, C. R. Acad. Sci. Paris 323 (1) (1996) 77–84.
[22] T. Gallouët, J.-M. Hérard, N. Seguin, Numerical modeling of two-phase flows using the two-fluid two-pressure approach, Math. Models Meth. Appl. Sci. 14 (5) (2004) 663–700.
[23] R. Panescu, Modélisation Eulérienne d'écoulements diphasiques à phase dispersée et simulation numérique par une méthode volumes – éléments finis, Mathématique appliquées, Université de Nice Sophia Antipolis, 2006.
[24] A. Harten, P. Lax, B. van Leer, On upstream differencing and Godunov-type schemes for hyperbolic conservation laws, SIAM Rev. 25 (1) (1983) 35–61.
[25] R. Eymard, T. Gallouët, R. Herbin, The finite volume method, in: P. Ciarlet, J.L. Lions (Eds.), Handbook for Numerical Analysis, North Holland, 2000.
[26] L. Gastaldo, R. Herbin, J.-C. Latché, Personal communication.
[27] M. Schwarz, Simulation of gas injection into liquid melts, Appl. Math. Modelling 20 (1996) 41–51.
[28] A. Sokolichin, G. Eigenberger, A. Lapin, Simulation of buoyancy driven bubbly flow: established simplifications and open questions, AIChE J. 50 (1) (2004) 24–45.
[29] N. Zuber, J.A. Findlay, Average volumetric concentration in two-phase flow systems, J. Heat Transfer (1965) 453–468.
[30] H. Paillère, C. Corre, J. Garcia Cascales, On the extension of the AUSM+ scheme to compressible two-fluid models, Comput. Fluids 32 (2003) 891–916.
[31] H. Staedtke, G. Franchello, B. Worth, U. Graf, P. Romstedt, A. Kumbaro, J. Garcìa-Cascales, H. Paillère, H. Deconinck, M. Ricchiuto, B. Smith, F. De Cachard, E. Toro, E. Romenski, S. Mimouni, Advanced three-dimensional two-phase flow simulation tools for application to reactor safety (astar), Nucl. Eng. Des. 235 (2-4) (2005) 379–400.
[32] F. Coquel, K. El Amine, E. Godlewski, B. Perthame, P. Rascle, A numerical method using upwind schemes for the resolution of two-phase flows, J. Comput. Phys. 136 (1997) 272–288.
[33] T. Gallouët, J.-M. Hérard, N. Seguin, On the use of symmetrizing variables for vacuums, Calcolo 40 (2003) 163–194.